Modeling of a Focused Gaussian Beam into Multi-Layered Tissue with Monte Carlo Simulation

Islam Saleh Attia El Ghargomi

A Thesis

In

The Department

of

Electrical and Computer Engineering

Presented in Partial Fulfillment of the requirements
For the Degree of Master of Applied Science (Electrical and Computer Engineering) at
Concordia University
Montreal, Quebec, Canada

December 2004

Your file Votre référence
ISBN: 0-494-04366-0
Our file Notre référence
ISBN: 0-494-04366-0

ABSTRACT

Modeling of a Focused Gaussian Beam into Multi-Layered Tissue with Monte Carlo Simulation

Islam Saleh Attia El Ghargomi

Monte Carlo method is a statistical method that is built on random sampling of variables from well-defined probability distributions. It has been employed rigorously to study the photon transport in biologically turbid media. This thesis employs a well-established simulation program called "MCML" to study photon transport in biologically turbid media. In the present work, we use Monte Carlo method for modeling finite diameter optical beams, which are in general approximated by uniform or Gaussian intensity distributions.

In order to model focused Gaussian beams with Monte Carlo simulation, the "MCML" program was modified based on a probability distribution found in the literature. However, errors were encountered in the calculated physical quantities by Monte Carlo simulation. This error formed a strong motivation to search for and analyze its source.

Using simulation, we prove that the probability density function used in the literature is a source of error in the calculations of the physical quantities evaluated by Monte Carlo simulation. We propose another probability density function that is shown to provide a dramatic improvement compared with the other function.

ACKNOWLEDGEMNTS

I would like to express appreciation to Dr. John Xiupu Zhang for giving me the chance to explore the interesting world of biophotonics; Endless thanks to Dr. O. Aboul-Atta for the fruitful discussion of convolution and valuable comments on the thesis; to my friend Hesham Elbatouti for answering my questions in programming; to my friend Diaa Nassar for his help in the final revision of the thesis; to my French teacher and friend Maamar Bouchouka for his continuous encouragement and help; to my wife Rasha for her love and support; to my lovely little daughter Mariam for her sweet smile and sense of humor; to my brother Ayman for always being ready to help; to my father and mother in law for their support; and finally, infinite gratitude to my parents for everything they have done for me.

Dedicated To

My Parents

Saleh El Ghargomi & Thanaa Aboul-Atta

Table of Contents

List of Figures

List of Tables

List of Symbols

μ_a	Absorption coefficient [cm^{-1}]
μ_s	Scattering coefficient [cm^{-1}]
g	Anisotropy factor [dimensionless]
θ	General Angle[radian]
n	Refractive index of the medium [dimensionless]
R	Fresnel's Reflectance [dimensionless]
λ	Wavelength of the light [cm]
ψ	Azimuth deflection angle after a single scattering event [radian]
$p(\theta)$	scattering function
d	Layer thickness [cm]
χ	Random variable
ξ_1	Uniformly distributed random number between (0,1)
$F(\chi)$	Cumulative distribution function of the random variable χ
f	Focal length of the focusing lens [cm]
I_o	Gaussian beam optical intensity at the beam center [$Watt/cm^2$]
W_o	Waist radius of a Gaussian beam [cm]
r	Radial distance in cylindrical coordinates [cm]
z	distance in the z-axis cylindrical coordinates [cm]
$W(z)$	Width or radius of a Gaussian beam at an axial distance z from the beam center [cm]
z_o	Rayleigh range of a Gaussian beam [cm]
P	Gaussian beam power [Watt]
W_o'	Waist radius of a Gaussian beam after focusing[cm]
z'	Axial distance from the lens of the focused Gaussian beam waist
b	Radius of uniform intensity photon beam [cm]
dr	Grid element separation in r direction [cm]
r_l	Radial launching position of photons [cm]
Φ	Radial angle [radian]
ζ	Random variable uniformly distributed between 0 and 1
ξ	Random variable uniformly distributed between 0 and 1
Z_f	Depth of focal point in the turbid medium [cm]
W_b	Normalized Gaussian beam radius by a factor of
u_x	Directional cosine in the x direction of the Cartesian coordinates [dimensionless]
u_y	Directional cosine in the y direction of the Cartesian coordinates [dimensionless]
u_z	Directional cosine in the z direction of the Cartesian coordinates [dimensionless]
n_m	Refractive index of medium
n_a	Refractive index of ambient

CHAPTER 1

Introduction

Biophotonics is the branch of science concerned with studying light interaction with biological matter [1]. Laser has shown applicability in the clinical domain as early as the 1960's [2]. The monochromatic, non-ionizing light can target and get absorbed by specific biomolecules, leaving others almost unaffected. The ability to focus laser beams into different spot sizes, which provides variable probing areas and consequently flexible delivery of radiation doses, is an important feature of laser. Guiding of laser beams using optical fibers, has made it possible to deliver optical energy *in vivo* to various organs in the human body with minimum invasion. This selectivity, minimally invasive, and relatively less harmful interaction between laser, and the biological tissues, makes laser an important clinical tool, both for diagnosis and therapy. The optimal treatment or diagnostic conditions for a certain tissue can be determined by choosing the appropriate

laser parameters such as intensity, irradiation geometry, operation wavelength, exposure time and exposure mode (pulsed or continuous) [3].

In terms of therapy, laser induces selective photobiological effects by transforming optical energy into chemical, thermal or mechanical energy via resonant light absorption [4]. Photo Dynamic Therapy (PDT), thermo therapy and tissue ablation are examples of the applications of laser in therapy. For diagnosis purposes, the analysis of reemitted and scattered light from tissue in terms of wavelength, temporal and spatial distributions, reveals important information about the optical properties of the biological tissue. diagnosis with laser involves non-destructive interaction between light and biological tissue. That is to say, absorption due to the incident optical power on tissue is below the threshold required to induce thermal and chemical reactions [3].

1.1 Scope of the Thesis

The theoretical models that were proposed to understand light transport in optically turbid biological tissues use the optical properties of tissue as inputs, in order to calculate the light distribution within the tissue or light escaping the tissue after interaction as the model output. One of the most famous modeling methods for light transport in optically turbid biological tissues is based on the radiative transfer equation [5,6]. The analytical solution of the radiative transfer equation is very complex and approximations are usually involved in the solution. Monte Carlo technique, first proposed by Metropolis and Ulam [7], simulates the radiative transfer equation by tracing a large number of statistical photons or energy packets each of which represents a fraction of the incident light energy [8-11]. The Monte Carlo method records photons histories as they are scattered and

absorbed. It is an attractive tool for modeling light transport in tissue because it can be easily implemented and can model complex tissue structures.

In this thesis, we present a Monte Carlo Model for a focused Gaussian beam into multi-layered biological tissue. We propose an accurate Monte Carlo sampling rule of the Gaussian beam profile and compare it with another sampling rule previously used in the literature. The Monte Carlo model for focusing a Gaussian beam is verified by means of comparison with simulation results in published reports. After verification of the model, we present the simulation results of two case studies, which involve focusing of a Gaussian beam into biologically turbid medium.

1.2 Organization of the Thesis

Chapter two reviews the fundamentals of tissue optics that are directly related to the research topic of the thesis. It also provides a short description of Monte Carlo simulation method for modeling light transport in multi-layered tissue. The main characteristics of Gaussian beams, which are modeled with Monte Carlo, are discussed at the end of this chapter.

Chapter three of this thesis concentrates on the details of the Monte Carlo model of a focused Gaussian beam into multi-layered tissue. A source of error in the sampling of a Gaussian beam profile, found in the literature, is highlighted and discussed. The derivation of the Monte Carlo sampling rule of both the uniform and Gaussian beam profiles is presented. The sampling rule of a beam profile refers to the random selection of the photon launching position within the beam radius that yields the required intensity profile in Monte Carlo simulation. The sampling rules of different beam profiles are

represented and discussed in sections (3.1) and (3.2). The method used to realize a focused optical beam in the Monte Carlo simulation model is discussed in Section (3.3).

The verification of the focused Gaussian beam model is presented in chapter four. This chapter is dedicated to verify the Monte Carlo simulation model by means of comparing the obtained results with those of published reports.

Chapter five introduces the application of the proposed model in two case studies. The first case involves focusing of a Gaussian beam into a homogeneous turbid medium and in the second case, into a human skin model consisting of two layers.

Finally, the main conclusions of the study, and the proposed future directions of research are presented in chapter six.

CHAPTER 2

Review of Literature

2.0 Biophotonics – A New Frontier

Biophotonics, or light interaction with biological matter, is an area of intensive scientific research. A multitude of applications of photonics in biology have emerged such as bioimaging, optical biosensors, light activated therapy, tissue engineering, laser tweezers, laser scissors and many other applications [1]. The understanding of the way laser interacts with biological tissues is the key to utilize laser both in diagnosis and therapy of diseases. The optically turbid biological tissue is characterized by its optical properties. These optical properties include the index of refraction, absorption coefficient, scattering coefficient, and scattering anisotropy [12]. The tissue optical properties are sensitive indicators of the biophysical status of biological tissue. The theoretical models that were proposed to understand light transport in optically turbid medium use the optical properties of tissue as inputs, in order to calculate the light distribution within the tissue or light escaping the tissue after interaction as the model output. The radiative transfer

equation [5] is one of the most famous modeling methods for light transport in optically turbid biological tissues [6]. This theory requires scatterers to be far enough away from each other to scatter independently from each other [13]. The analytical solution of the radiative transfer equation is very complex and approximations are usually involved in the solution. Therefore, other approaches rather than the analytical one are usually required in order to provide a solution for this equation. Monte Carlo technique simulates the radiative transfer equation by tracing a large number of statistical photons or energy packets each of which represents a fraction of the incident light energy [8-11]. It is a well-established tool that has proved to produce computation results that are closely corresponding to measured values [14].

In the next section a short description of the general aspects of light transport in tissue is presented. Then, the Monte Carlo method and its implementation to simulate photon propagation in multi-layered tissue are presented. The last part of this chapter discusses the main characteristics of a Gaussian beam, which are modeled with Monte Carlo simulation.

2.1 Tissue Optical Properties

Biological tissues are optically characterized by four important properties: the refractive index n (dimensionless), the absorption coefficient μ_a in cm^{-1}, the scattering coefficient μ_s in cm^{-1}, and the anisotropy factor g (dimensionless). In the following sections, a brief discussion of each one of these properties is presented.

2.1.1 The Refractive Index n

It is well known that the refractive index is defined as the ratio between the speed of light in vacuum to its speed in the medium. Therefore, the refractive index can be seen as the

resistance the light encounters during its propagation in the medium compared by its propagation in the free space. If light is incident on the interface between two media with different refractive indices, fraction of the incident light will suffer from specular reflection and fraction of the incident light will be transmitted into the second medium as a refracted beam according to Snell's law. Figure (2-1) shows the reflected and transmitted light at ambient-tissue boundary due to mismatched refractive indices between the two media [12].

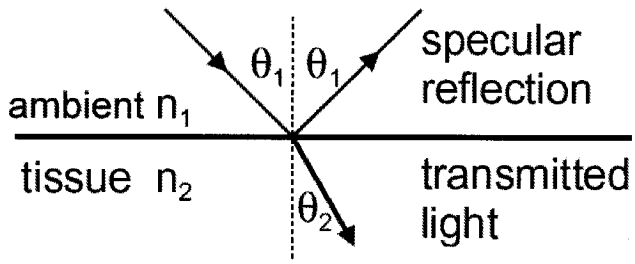

Figure (2-1) Reflected and transmitted light at ambient-tissue boundary due to mismatched refractive indices between the two media.

According to Snell's law of refraction:

$$n_1 \sin\theta_1 = n_2 \sin\theta_2 \qquad (2\text{-}1)$$

Where θ_1 is the angle of incidence with respect to the normal of the surface boundary, and θ_2 is the angle of transmittance measure from the same reference. The refractive indices of the first and second media are n_1 and n_2 respectively.

The specular reflection is governed by the Fresnel's formulas, and depends strongly on the angle of incidence, the polarization status of the incident light beam and the nature of the reflecting surface [12]. The reflectance R is given by Fresnel's formulas as[10-12,15]:

$$R = \frac{1}{2}\left[\frac{\tan^2(\theta_1-\theta_2)}{\tan^2(\theta_1+\theta_2)} + \frac{\sin^2(\theta_1-\theta_2)}{\sin^2(\theta_1+\theta_2)}\right] \qquad (2\text{-}2)$$

Equation (2-2) represents an average of the reflectances for the two orthogonal polarization directions. From equation (2-1) it can be seen that, if the angle of incidence on the tissue surface is equal to zero (i.e. normal incidence), then the angle of refraction will be also zero. In this case, equation (2-2) reduces to:

$$R = \left(\frac{n_2 - n_1}{n_2 + n_1} \right)^2 \tag{2-3}$$

2.1.2 The Absorption Coefficient μ_a

The absorption of photons by biological tissue is a very important event in biophotonics. It provides both therapeutic as well as diagnostic information regarding the biological tissue under study. In terms of therapy, absorption means energy transfer to the tissue and in terms of diagnostics, absorption provides information about the chemical composition of the tissue in spectroscopic applications. Absorption also acts as a contrast mechanism in imaging applications. The probability of absorption per unit path length of a traveling photon defines the absorption coefficient μ_a in cm^{-1} [16]. Figure (2-2) shows the primary absorption spectra of some biological tissues and the absorption coefficients at some typical wavelengths.

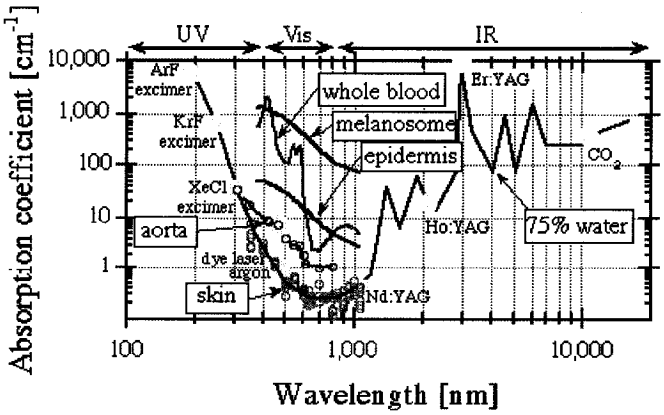

Figure (2-2) Primary absorption spectra of biological tissues and absorption coefficients at some typical laser wavelengths [16].

From figure (2-2) it can be seen that, the absorption increases in the ultraviolet region of the optical spectrum due to protein, Deoxyribonucleic Acid (DNA), and other molecules. In the infrared region, the absorption increases with increasing wavelengths mainly due to water absorption. The red to the near-infrared region is characterized by minimal absorption [16].

2.1.3 The Scattering Coefficient μ_s

The scattering coefficient is defined as the probability of photon scattering per unit path length μ_s in cm^{-1}. The summation of the scattering and absorption coefficients defines the total attenuation coefficient μ_a, which accounts for the probability of all light-tissue interactions per unit path length of a propagating photon. Photons propagating in optically turbid biological tissue with wavelengths close to the size of the tissue ultra structure will suffer strongly from scattering due to interaction with tissue ultra structure. The tissue ultra structure extends from membranes, to membrane aggregates, to collagen fibers, to nuclei, to cells [16]. Scattering can be referred to the small local variations in the mean real refractive index of the medium [17]. The scattering regime is highly dependent on the wavelength of the photon compared to the size of the scatterer. If the incident photon wavelength is in the order of size of the scattering structure, the scattering process is described by the Mie theory. If the scattering structure is very small in size compared to the incident photon wavelength, then the scattering process is best described by the Rayleigh scattering regime [12,16]. In the Rayleigh limit, the wavelength dependence on the scattering varies as λ^{-4} ,while for larger particle sizes it changes as λ^{-2}, where λ is the wavelength of the photon[15]. This means that red light is less scattered than blue light since the blue light has a shorter wavelength. It should be

noted that the term scattering used in this thesis refers only to elastic scattering where the incident and scattered photons have the same energy.

2.1.4 Scattering Anisotropy g

The anisotropy or asymmetry factor, also named the g-factor, is defined as the average cosine of the deflection angle θ at a single scattering event [18]. The angle θ is measured with respect to the original forward trajectory of the singly scattered photon. The graphical representation of the scattering deflection angle θ and the azimuth angle ψ due to a single scattering event is shown in figure (2-3).

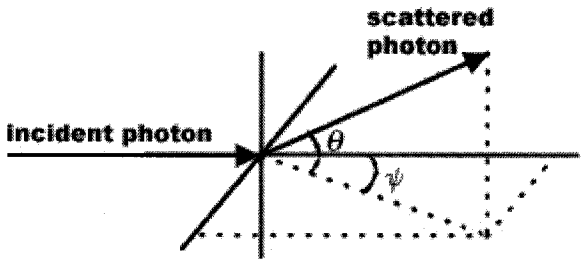

Figure (2-3) Graphical representation of the deflection and azimuth angles after a photon suffers from a single scattering event.

If the scattering tissue has no major regions that can be regarded as organized structure, (i.e. the scattering medium is considered isotropic), then the azimuth angle ψ will be uniformly distributed between 0 and 2π. The deflection angle θ falls within the range 0 and π. The anisotropy factor g is actually a measure of the amount of forward direction retained after a single scattering event. The angular dependence of scattering which is called the scattering function $p(\theta)$, is described by the probability of a photon scattering into a unit solid angle oriented at an angle θ relative to the original photon trajectory [18]. In other words, the scattering function describes the intensity of light scattered from an object as a function of the angle between the incident direction and the scattered direction

[19]. In tissue optics, the Henyey-Greenstein phase function [20] has proven to be useful in approximating the angular dependence of single scattering events in biological tissues [19-21]. The Henyey-Greenstein phase function is given by:

$$p(\theta) = \frac{1}{4\pi} \frac{1-g^2}{(1+g^2-2g\cos\theta)^{3/2}} \tag{2-4}$$

such that, $\int_0^{\pi} p(\theta) 2\pi \sin(\theta) d\theta = 1$, and $\int_0^{\pi} p(\theta)\cos(\theta) 2\pi \sin(\theta) d\theta = g$

It is common to write the Henyey-Greenstein as a function of *P(cosθ)* :

$$P(\cos\theta) = \frac{1}{2} \frac{(1-g^2)}{(1+g^2-2g\cos\theta)^{3/2}} \tag{2-5}$$

such that $\int_{-1}^{1} P(\cos\theta) d(\cos\theta) = 1$ and $\int_{-1}^{1} P(\cos\theta)\cos(\theta) d(\cos\theta) = g$.

The scattering anisotropy g = <cosθ>,(meaning, the expected value of cosθ) , and has a value between -1 and 1.

A g-factor close to zero means that the scattering is isotropic, while a value close to unity indicates a sharply scattering peak in the forward direction. Most biological tissues have, in general, a forward directed scattering [19,21,22].

2.2 Monte Carlo Simulation Method for Modeling Light Transport in Multi-Layered Tissue

Monte Carlo methods are used for solving widely varying types of physical problems. Surprisingly, there is no well-established definition for this method. A good definition is presented by Lux and Koblinger [23] as: "In all applications of the Monte Carlo method, a stochastic model is constructed in which the expected value of a certain random variable (or a combination of random variables) is equivalent to the value of a physical quantity to be determined. This expected value of the random variable is estimated by the

average of multiple independent samples representing the random variable introduced above. For the construction of the series of independent samples, random numbers following the distribution of the variable to be estimated are used". Kahn published the first comprehensive review about Monte Carlo methods in 1954 [24]. Monte Carlo method has been employed rigorously to study the photon transport in turbid medium. The MCML [25,26] Monte Carlo simulation program of steady state light transport in multi-layered tissues is a well-established simulation tool in this domain. It deals with the transport of an infinitely narrow photon beam perpendicularly incident on a multi-layered tissue. The MCML computer simulation program was modified to fit the needs of the research topic in this thesis, specifically to model optical beams of finite diameters with different intensity profiles (uniform or Gaussian) when focused into multi-layered tissue. The Monte Carlo simulation program models an incident photon beam on infinitely wide multi-layered tissue. Each tissue layer is characterized by its thickness, refractive index, absorption coefficient, scattering coefficient, and anisotropy factor. Also the top and bottom ambient refractive indices are needed to complete the simulation model input information. The aim of the simulation is to predict the radiant energy transport in the turbid tissue. The simulation does not treat the photon as wave phenomena, but rather as energy packets. Therefore all phase and polarization features are ignored in the Monte Carlo simulation. Since Monte Carlo methods are statistical in nature, they require a large number of photons to be traced in each simulation run and therefore it is a time consuming method in general. The number of photons to be used in the simulation run depends on the required accuracy, spatial resolution needed and the quantity that is being measured. The outputs of the simulation are four physical quantities of interest: photon

absorption, fluence, reflectance and transmittance. In order to score these important physical quantities in the three-dimensional space, a special grid system in space is constructed for this purpose. Three simultaneous coordinate systems are used in the Monte Carlo simulation. A Cartesian coordinate system traces the photon movement. To score internal photon absorption, a cylindrical coordinate system is setup for this purpose since the problem has cylindrical symmetry. The diffuse reflectance and transmittance emerging out of the tissue are also recorded in the cylindrical coordinate system as a function of the radial distance and the angle between the photon exiting direction and the normal to the surface. It should be noted that both the Cartesian coordinate system and the cylindrical coordinate system share the same z-axis and the point of origin. A third spherical coordinate system is used to sample the propagation direction change of the photon packet. The reader is strongly advised to read references [10,11,25,26] in order to understand the principles of Monte Carlo simulations for photon transport in tissue, as it is not possible to discuss all details in this thesis. However, some of the Monte Carlo principles that are directly related to the research point in this thesis will be discussed in more detail. Figure (2-4) below shows the flow chart for Monte Carlo simulation of photon propagation in multi-layered tissue [25,26]. It should be mentioned that the MCML computer program is associated with another program called "CONV" [27] for solving responses due to a collimated finite diameter photon beam perpendicularly incident on multi-layered tissue. The CONV program employs an extended trapezoidal rule for integration, to convolve the responses to an infinitely narrow photon beam computed by the MCML program. Unfortunately, The CONV program can not calculate the responses due to beams of finite diameters other than normally incident beams.

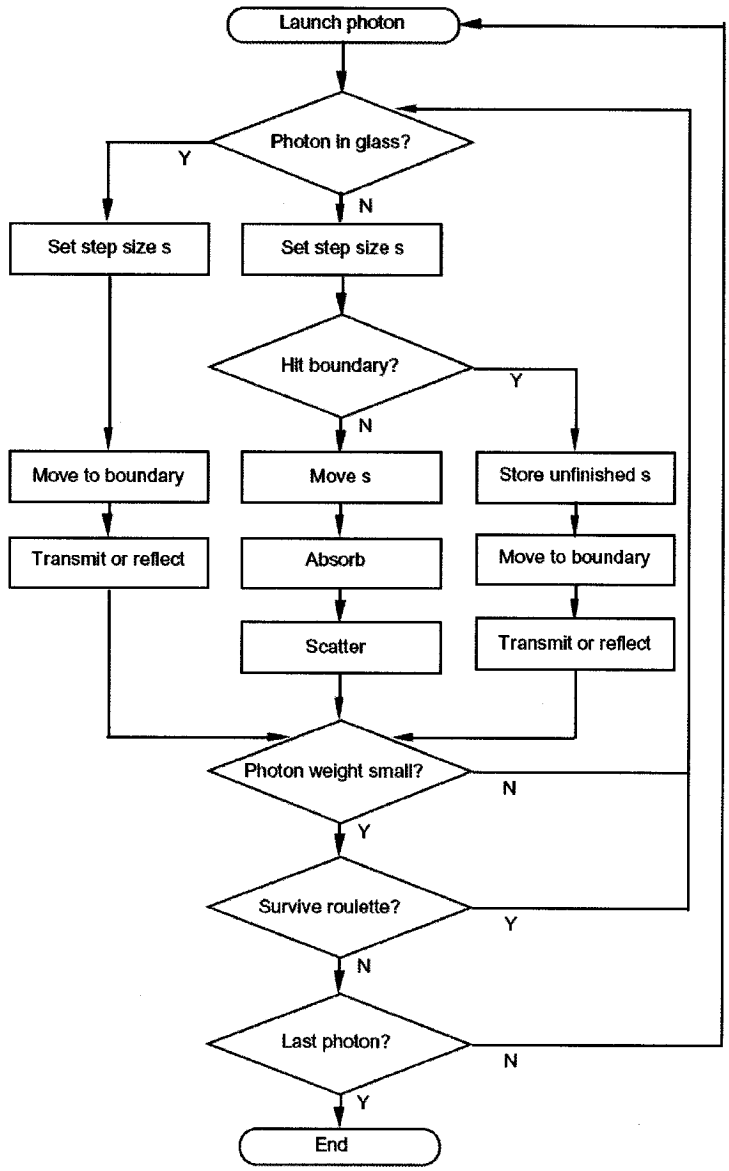

Figure (2- 4) Flow chart for Monte Carlo simulation of photon propagation in multi-layered tissue [25,26].

2.2.1 Sampling of Random Variables in Monte Carlo Simulation

Monte Carlo method is a statistical method that is built on random sampling of variables from well-defined probability distributions. Due to the importance of this procedure, a review is presented here according to references [10,23,25,26,28]. Consider a random variable χ which represents a random variable of interest in the Monte Carlo simulation such as the random step size between two successive interaction sites, or the random

deflection angle after a single scattering event, etc. The normalized probability density function that defines the distribution of χ over the interval (a,b) is p(χ) such that:

$$\int_a^b p(\chi)d\chi = 1 \qquad (2\text{-}6)$$

It is desirable to be able to choose a value for χ repeatedly and randomly based on a pseudo-random number generator to simulate the propagation process of the photon. The computer provides a random variable, ξ, which is uniformly distributed over the interval (0, 1). The cumulative distribution function of this uniformly distributed random variable is then given by:

$$F_\zeta(\xi) = \begin{cases} 0 & \text{if } \xi \le 0 \\ \xi & \text{if } 0 < \xi < 1 \\ 1 & \text{if } \xi > 1 \end{cases} \qquad (2\text{-}7)$$

In order to sample a non-uniformly distributed function $p(\chi)$, we assume there exists a non decreasing function $\chi = f(\xi)$, which maps $\xi \in (0, 1)$ to $\chi \in (a, b)$. The variable χ and variable ξ then have a one-to-one mapping. According to the definition of cumulative distribution functions, and equation (2-7), it can be shown that:

$$F_\chi(\chi_1) = F_\xi(\xi_1) \qquad (2\text{-}8)$$

Expanding the left hand side of equation (2-8) using the definition of cumulative distribution function, and substituting equation (2-7) into the right hand side of equation (2-8), we get:

$$\int_a^{\chi_1} p(\chi)d\chi = \xi_1 \qquad \text{for } \xi_1 \in (0,1) \qquad (2\text{-}9)$$

Equation (2-9) is then solved to get the value of χ_1. This solution for χ_1 is equivalent to transforming the random variable ξ_1 into χ_1 through the function $\chi = f(\xi)$. Equation (2-9) is the basic equation in sampling propagation variables in Monte Carlo simulation. Each

time a new random value of any propagation variable needs to be generated; this equation is used during the Monte Carlo simulation process. Figure (2-5) shows the graphical representation of sampling a random variable χ based on a uniformly distributed computer generated random variable ξ.

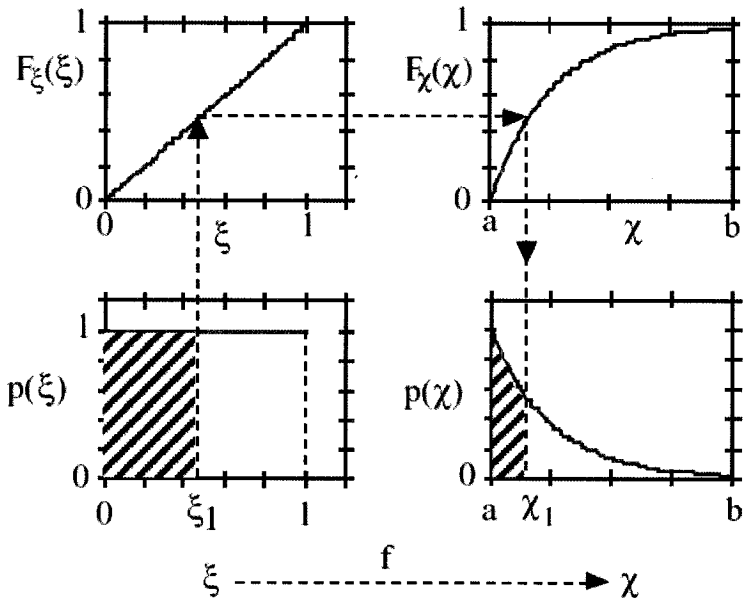

Figure (2- 5) Sampling a random variable χ based on a uniformly distributed random variable ξ [26].

It should be noted that, since for each ξ_i, a χ_i is chosen such that the cumulative distribution functions for ξ_i and χ_i have the same value. Therefore, the hatched areas shown in figure (2-5) are equal.

2.3 Gaussian Beams

The discussion in this section focuses mainly on the fundamental characteristics of Gaussian beams, which are discussed in more details in references [29,30]. This review concentrates on the characteristics that are relevant to the topic of this thesis.

2.3.1 General Characteristics of a Gaussian Beam

Within the paraxial wave approximation [29], beams originating from laser sources can be represented by Gaussian beams [30]. Let's assume that we have a Gaussian laser beam traveling along the positive z-axis, the optical intensity of a Gaussian beam is a function of both the axial and radial distances z and r respectively, and is given by:

$$I(r,z) = I_o\left[\frac{W_o}{W(z)}\right]^2 \exp\left[-\frac{2r^2}{W^2(z)}\right] \tag{2-10}$$

where I_o is Gaussian beam optical intensity at the beam center in watt/cm^2, W_o is waist radius of the Gaussian beam in cm, r is the radial distance in the transverse plane measured from the beam center in cm, and $W(z)$ is the width or radius in cm of the Gaussian beam at an axial distance z. The beam width $W(z)$ of the Gaussian beam is defined as the radius at which the intensity drops to $1/e^2$ of its peak value at the beam center. The width of the Gaussian beam as a function of the axial distance z is given:

$$W(z) = W_o\left[1+(\frac{z}{z_o})^2\right]^{\frac{1}{2}} \tag{2-11}$$

where z_o is the Rayleigh range of the Gaussian beam in cm. The relation between the waist radius W_o and the Rayleight range of a Gaussian beam is given by:

$$W_o = (\frac{\lambda z_o}{\pi})^{\frac{1}{2}} \tag{2-12}$$

The same equation can be written as:

$$z_o = \frac{\pi W_o^2}{\lambda} \tag{2-13}$$

where λ is the wavelength of the used light source. The waist radius W_o is the minimum value of beam radius $W(z)$ in the plane z =0 as seen from equation (2-11).The total optical power contained in the beam is given by:

$$P = \frac{1}{2} I_o(\pi W_o^2) \tag{2-14}$$

From equation (2-14), it can be seen that the beam power is independent of the axial distance z. Since the beam radius has a minimum at the plane z =0, then it is expected that the beam achieves its best focus at this specific plane. The depth of focus of a Gaussian beam is then defined as the axial distance within which the beam radius lies within a factor of $\sqrt{2}$ of its minimum value as shown in figure (2-6).

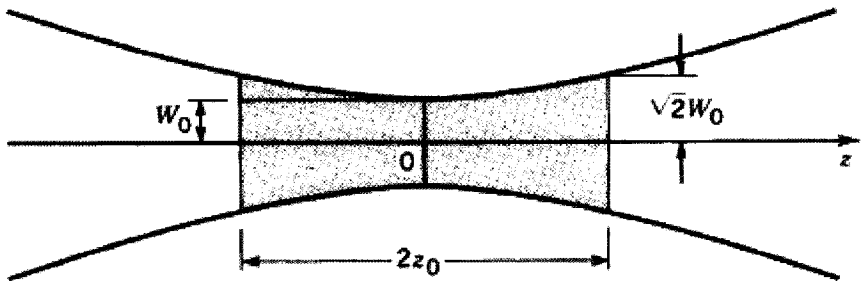

Figure (2-6) Depth of focus of a Gaussian beam [30]

Another important characteristic of the Gaussian beam is that the wave front at the axial distance z = 0 is a planar wave front. Generally the wave fronts near the center of the beam within the Rayleigh range can be approximated by planar wave fronts [30]. The value of this feature will be clear soon as we discuss the focusing of Gaussian beams using thin lenses.

2.3.2 Focusing of a Gaussian Beam using a Thin Lens

It can be proved that a Gaussian beam transmitted through a thin lens remains Gaussian as well [30]. If a thin focusing lens is placed at the waist of a Gaussian beam traveling in

the positive z-direction, then the transmitted beam is focused at a distance z' from the lens and to a new waist radius W_o' given by:

$$W'_o = \frac{W_o}{[1+(\frac{z_o}{f})^2]^{\frac{1}{2}}} \tag{2-16}$$

$$z' = \frac{W_o}{[1+(\frac{f}{z_o})^2]} \tag{2-17}$$

where z_o is the Rayleigh range of a Gaussian beam in cm, and f is the focal length. The focusing of a Gaussian beam by a thin lens placed at the beam waist is shown in figure (2-7) below.

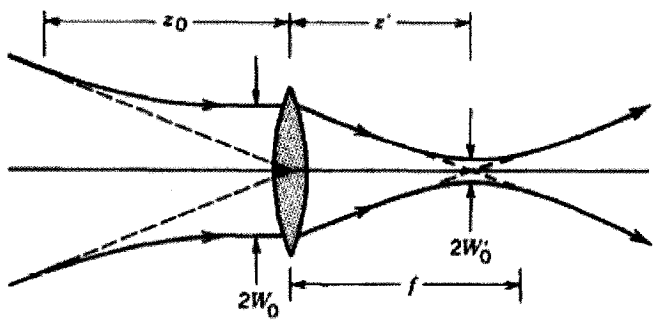

Figure (2-7) Focusing a Gaussian beam using a thin lens placed at the beam waist [30].

If the depth of focus of the incident beam $2z_o$, is much longer than the focal length f of the lens as seen in figure (2-7), then:

$$W'_o \approx (\frac{f}{z_o}) \tag{2-18}$$

Using equation (2-13), the following relations are easily obtained:

$$W'_o \approx \frac{\lambda}{\pi W_o} f \tag{2-19}$$

$$z' \approx f \tag{2-20}$$

Therefore, a Gaussian beam transmitted through a thin lens placed at its waist will be focused at the lens' focal plane as would be expected for a collimated beam incident on the same lens. It is important to notice that these relations are valid only when the Gaussian beam is focused at its beam waist. In the model presented in the next chapter, these assumptions were made. The focusing lens is placed at the beam's waist and the Rayleigh range of the beam is much larger than the focal length of the used lens.

2.4 Summary

In this chapter, a review of the fundamentals of tissue optics that are directly related to the thesis topics is presented. Also a short description of Monte Carlo method for simulating light transport in multi-layered tissue is given. Finally the main characteristics of Gaussian beams are discussed at the end of this chapter.

CHAPTER 3

Monte Carlo Modeling of a Focused Gaussian Beam Into Multi-Layered Tissue

3.0 Problem Statement and Research Objectives

This chapter presents the Monte Carlo Model for analyzing light propagation in multi-layered tissue due to a focused Gaussian beam. The main goal of the study of laser–tissue interaction is to understand and to simulate light transport in optically turbid biological tissues by use of various theoretical models. As mentioned before, the Monte Carlo technique simulates the radiative transfer equation by tracing a large number of statistical photons or energy packets each of which represents a fraction of the incident light energy. Each layer is characterized by the five parameters: layer thickness d, refractive index n, the absorption coefficient μ_a, the scattering coefficient μ_s and anisotropy factor g. In order to build a Monte Carlo model for a focused Gaussian beam propagating in optically turbid biological tissue, the search for a well-established modeling tool was essential. The MCML [25], program that is written in standard C language, represented

an excellent start point in the quest for a modeling tool. The program is being used widely in modeling light transport in tissue. It has been proved to produce results that match with the measured physical quantities [14]. This simulation tool, including source code, is available for free download from the authors' academic institutions' web sites. The MCML computer program calculates the response due to an infinitely narrow photon beam perpendicularly incident on a multi-layered tissue. Unfortunately, it neither models finite diameter optical beams, nor the focusing process. The MCML source code was modified in order to allow modeling of a Gaussian beam (or uniform intensity beam) with a known beam radius to be focused into the multi-layered tissue under study. The modifications that we implemented in the program can be summarized in two main points: First, we had to make the program sample a probability density function that best describes a Gaussian (or uniform) intensity profile. Second, we had to program the launching method of photons according to the selected criterion of focusing, taking into account the spatial properties of the focusing method used. The explanation of the Monte Carlo method of sampling beam profiles, both uniform and Gaussian, is discussed in sections 3.1 and 3.2. The method of realizing the focusing process in the model is presented in section 3.3. We must mention that during the modeling of the focused Gaussian beam, we first used a probability density function that is found in the literature [31,32]. This probability density function, which is said to represent a Gaussian beam profile in Monte Carlo simulation of light transport in tissue, caused unacceptable errors in the calculated physical quantities that were as big as 50% in some cases. This was a big motive for us to make a derivation of the sampling rule that best characterizes the Gaussian beam profile and compare it with the one found in the literature to explain the

source of this error. This derivation is shown in section 3.2 as mentioned before. We must highlight that references [31,32] neither introduced a derivation of the probability density function they used, nor they referred to the source of this probability function. We will prove in section 3.2 that our proposed probability density function, which is derived in detail, accurately resembles a Gaussian beam profile better than the one proposed by [31,32]. In the next chapter that we verify and compare the behavior of the two probability functions by running the Monte Carlo simulation model.

3.1 Monte Carlo Sampling of a Uniform Intensity Beam Profile

A uniform intensity profile of an optical beam of finite size is an idealized description of light emerging from laser sources. Normally, laser sources can be approximated by Gaussian beams within the paraxial regime as mentioned in the previous chapter. To simulate the launching of a collimated photon beam of uniform intensity profile, the launching position of the photon packets must be randomly selected so that a uniform spatial distribution of photon launching is achieved [16]. Now, consider the uniform intensity optical beam of radius b cm. The beam is incident normally on the tissue towards the positive z-axis of the Cartesian coordinates. The normalized intensity in cm^{-2} of the beam is given by:

$$I(r) = \frac{1}{\pi b^2} \tag{3-1}$$

The probability density function describing the beam profile as a function of r is then given by:

$$p(r) = \frac{2\pi r}{\pi b^2} = \frac{2r}{b^2} \qquad \text{such that,} \quad \int_0^b p(r)dr = 1 \tag{3-2}$$

where the term $(\frac{1}{\pi b^2})$ describes the radial dependence of the beam intensity. The second term $(2\pi r)$ describes the circular rings of integration over the cross section of the beam. Applying the Monte Carlo method of sampling the probability distribution function of random variables of interest using a computer generated random variable which is uniformly distributed between 0 and 1 inclusive [10,25,26] and described in section (2.2.1), the cumulative distribution function of the random variable r at $r = r_l$ is given by:

$$F(r_l) = \int_0^{r_l} p(r)dr = \frac{r^2}{b^2} = \xi_l \tag{3-3}$$

which leads to the sampling rule of selecting the radial launching position r_l based on the randomly generated variable ξ_l where $\xi_l \in (0,1)$:

$$r_l = b\sqrt{\xi_l} \tag{3-4}$$

In order to determine completely the photon launch position, the determination of the radial angle Φ in the x-y plane is also necessary. The radial angle Φ is measured with respect to the x-axis in the x-y plane as shown in figure (3-1) below.

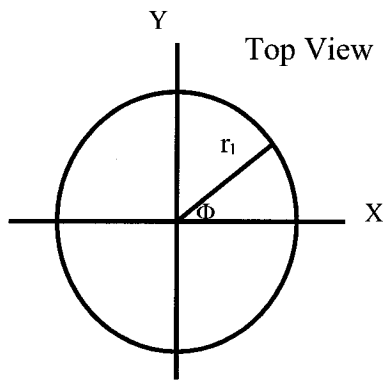

Figure (3-1) Selection of photon launching position in Monte Carlo simulation. The radial position $r_l$and the radial angle Φ specify the exact position of the photon to be launched. The x-y plane is the plane of the tissue surface.

The radial angle Φ, which is determined by generating a second random number ζ uniformly distributed between 0 and 1 inclusive, is determined by randomly selecting an angle between 0 and 2π inclusive, therefore:

$$\Phi = 2\pi\zeta \tag{3-5}$$

where $\zeta \in (0,1)$

The Cartesian coordinates of the photon launching position can be easily determined accordingly:

$$x = r_l \cos\Phi \tag{3-6}$$

$$y = r_l \sin\Phi \tag{3-7}$$

Equations (3-4) to (3-7) define the sampling rule of a uniform intensity beam profile in Monte Carlo simulation.

It is required now to verify that equation (3-4), which describes the random radial launching position of Monte Carlo photons, will yield a uniform intensity beam profile. A short MATLAB program [16] was used to verify equation (3-4). The steps to generate the intensity profile resulting from equation (3-4) are as follows: One million randomly generated numbers $\{\xi_l$ in equation (3-4)$\}$ are used to construct a normalized histogram of the random variable r_1. The histogram then represents the probability density function describing the radial launching position of a photon within a uniform intensity beam profile $p(r)$. The computer generated intensity profile of the beam is obtained by dividing $p(r)$ by $2\pi r$ according to equations (3-1) and (3-2). Figure (3-2) shows the resulting intensity profile as generated by the computer when plotted against the analytical expression of a uniform intensity profile given by equation (3-1). It can be noticed that the computer generated intensity profile based on equation (3-4) is matching the

analytical expression given by equation (3-1). It is clear from figure (3-2) that the sampling rule described by equations (3-4) to (3-7), represents a uniform intensity beam profile as expected.

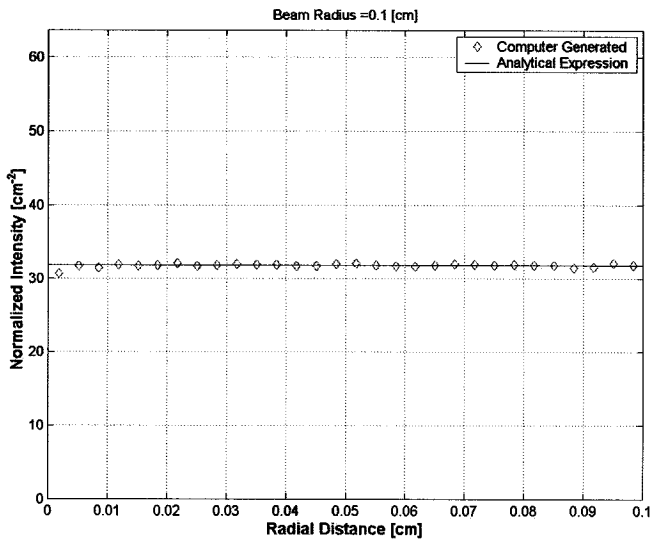

Figure (3-2) Normalized uniform intensity beam profile of 0.1 cm radius

3.2 Monte Carlo Sampling of a Gaussian Beam Profile

In this section we present the detailed derivation of the Monte Carlo sampling rule. We believe that this rule describes accurately a Gaussian beam profile in comparison with the one proposed in references [31,32] without proof. The derivation of the sampling rule starts from the well-known intensity profile of a Gaussian beam because Monte Carlo method for analyzing light transport in tissue is based on tracing multitude photons representing energy packets [8-11]. As it is known, the Gaussian beam power is principally concentrated within a small cylinder surrounding the beam axis. The intensity distribution in any transverse plane is a circularly symmetric Gaussian function centered about the beam axis [30]. Equation (2-10) in the previous chapter describes the optical intensity of a Gaussian beam as a function of the axial and radial distances. Now consider

the axial plane where $z = 0$. At this plane the width of the beam is minimum and is called the beam waist W_o. At this plane the optical intensity is given by:

$$I(r) = I_o \exp\left[-\frac{2r^2}{W_o^2}\right] \tag{3-8}$$

Using equation (2-14) and considering the total beam power P =1 watt, then substitute I_o in equation (3-8):

$$I(r) = \frac{2}{\pi W_o^2} \exp\left[\frac{-2r^2}{W_o^2}\right] \tag{3-9}$$

The probability density function describing the Gaussian beam profile as a function of r is then given by:

$$p(r) = \frac{2}{\pi W_o^2} \exp\left[\frac{-2r^2}{W_o^2}\right].2\pi r \text{ , such that } \int_0^\infty p(r)dr = 1 \tag{3-10}$$

where, the first term of equation (3-10) describes the radial dependence of the beam intensity, while the second term ($2\pi r$) describes the circular rings of integration over the cross section of the beam. Equation (3-10) is rewritten as:

$$p(r) = \frac{4r}{W_o^2} \exp\left[\frac{-2r^2}{W_o^2}\right] \text{ , Such that } \int_0^\infty p(r)dr = 1 \tag{3-11}$$

Applying the Monte Carlo method of sampling the probability distribution function of random variables of interest described in section (2.2.1), the cumulative distribution function of the random variable r at $r = r_1$ is given by:

$$F(r_1) = \int_0^{r_1} p(r)dr = \left[1 - \exp\left(\frac{-2r_1^2}{W_o^2}\right)\right] = \xi_1 \tag{3-12}$$

which leads to the sampling rule of selecting the radial launching position r_1 based on the randomly generated variable ξ_1, where $\xi_1 \in (0,1)$:

$$r_1 = \frac{W_o}{\sqrt{2}}\sqrt{-\ln(1-\xi_1)} \tag{3-13}$$

Since ξ_1 is a random number uniformly distributed between 0 and 1 inclusive, then $(1-\xi_1)$ will also be a random number uniformly distributed between 0 and 1 inclusive. As a result, the term $ln(1-\xi_1)$ in equation (3-13) is equivalent to the term $ln(\xi_1)$. Then, equation (3-13) can be written as:

$$r_1 = \frac{W_o}{\sqrt{2}}\sqrt{-\ln(\xi_1)} \tag{3-14}$$

The sampling rule given by equation (3-14) will be denoted as "sampling rule I". In order to completely determine the photon launch position, the determination of the radial angle Φ in the x-y plane is also necessary. The radial Φ is measured with respect to the x-axis in the x-y plane as shown in figure (3-1). The radial angle Φ, which is determined by generating a second random number ζ uniformly distributed between 0 and 1 inclusive, is determined by randomly selecting an angle between 0 and 2π inclusive, therefore, Φ is sampled according to equation (3-5). Similar to the case of the uniform intensity beam discussed in section (3-1), the Cartesian coordinates of the photon launching position can be easily determined according to equation (3-6). Equations (3-5) to (3-7) and equation (3-14), all define the sampling rule of a Gaussian beam profile in Monte Carlo simulation.

It is required to verify that equation (3-14) yields probability density function described by equation (3-11), and the Gaussian intensity profile described by equation (3-9). A short MATLAB program [16] was used to build the probability density function based on one million randomly generated numbers in equation (3-14). The obtained results are shown in figures (3-3) and (3-4). The $1/e^2$ beam radius was taken to be 0.1 cm as this

radius is relevant to the cases studied by simulation in chapter four. Figure (3-4) shows the intensity profile of the beam as generated by sampling rule I. Figure (3-4) represents a Gaussian intensity profile with $1/e^2$ beam radius of 0.1 cm as expected.

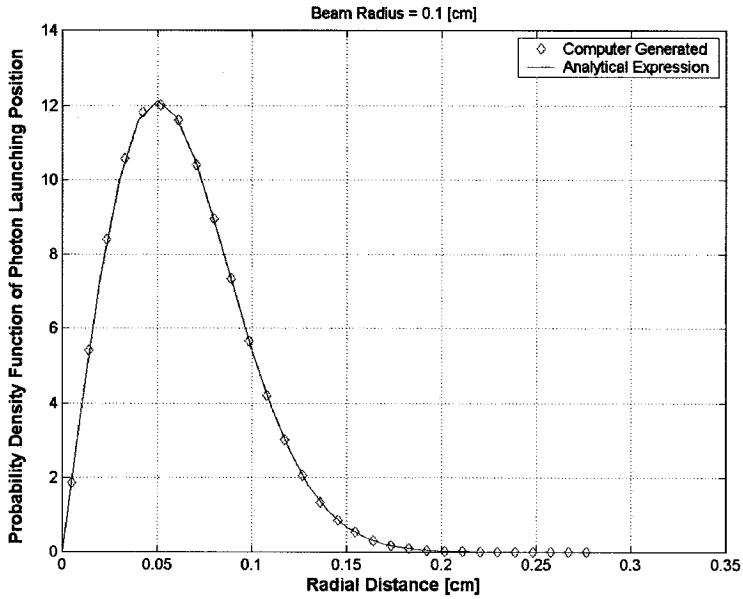

Figure (3-3) Probability density function of photon radial launching position of a Gaussian beam profile with $1/e^2$ radius of 0.1 cm according to sampling rule I.

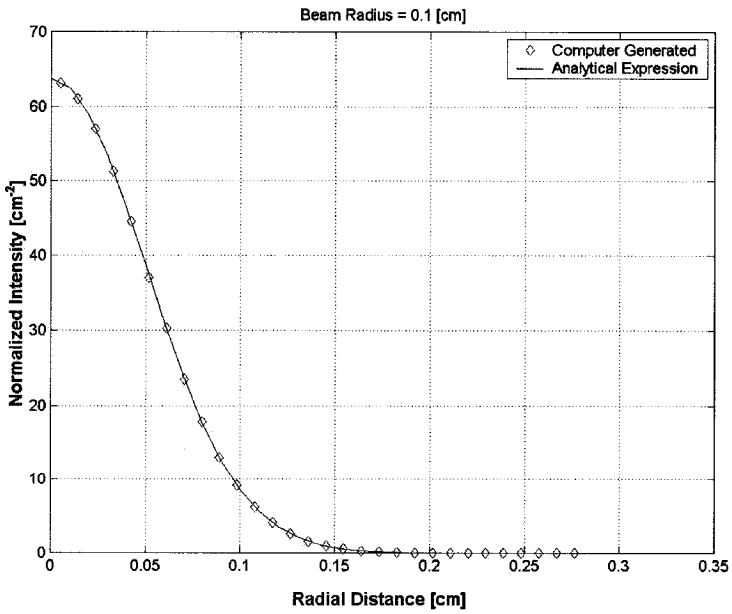

Figure (3-4) Normalized intensity profile of a Gaussian beam with $1/e^2$ radius of 0.1 cm, according to sampling rule I

In the literature however, some references [31,32] used another probability density function rather than the one mentioned in equation (3-11) to describe a Gaussian beam profile as a function of radial distance in Monte Carlo simulation of light transport in tissue. References [31,32] used the probability density function given by:

$$p(r)=\frac{2r}{W_b^2}\exp\left[\frac{-r^2}{W_b^2}\right], \text{ such that } \int_0^\infty p(r)dr=1 \tag{3-15}$$

where W_b was defined as the "Gaussian beam width" in references [31,32] which is also called the beam radius. Following the same steps for sampling the probability density. Following the Monte Carlo method of sampling the probability density function of random variables that is mentioned in section (2.2.1) leads to the sampling rule for selecting the photon launching at radial position r_l based on the randomly generated variable ξ_l, where $\xi_l \in (0,1)$:

$$r_l=W_b\sqrt{-\ln(\xi_l)} \tag{3-16}$$

The sampling rule given by equation (3-16) will be denoted as sampling rule II for the purpose of comparison with equation (3-14). It is clear that the definition of W_b in the literature as the "Gaussian beam width" is inaccurate. W_b is the normalized beam waist by a factor of $\sqrt{2}$. The implementation of the sampling rule suggested by equation (3-16) when taking W_b as the beam radius leads to a considerable error in the calculation of all the physical quantities scored in Monte Carlo simulation. This conclusion can not be considered trivial because, as we will see in the next chapter, the application of sampling rule II without correction of W_b parameter will lead to an error in the calculated physical quantities by Monte Carlo simulation that approaches 50% in some cases. Comparing equations (3-14) and (3-16), the relation between the W_o and the parameter W_b can be

written as $W_b = \frac{W_o}{\sqrt{2}}$. Therefore we expect the error resulting from sampling rule II to be dependent on the actual waist radius W_o. In other words, if the beam waist W_o is very small, the resulting error due to the use of W_b in the simulation instead of W_o is expected to be very small and vice versa. A plot of the probability density function given by equation (3-15) and the generated probability density function by equation (3-16) is shown in figure (3-5).

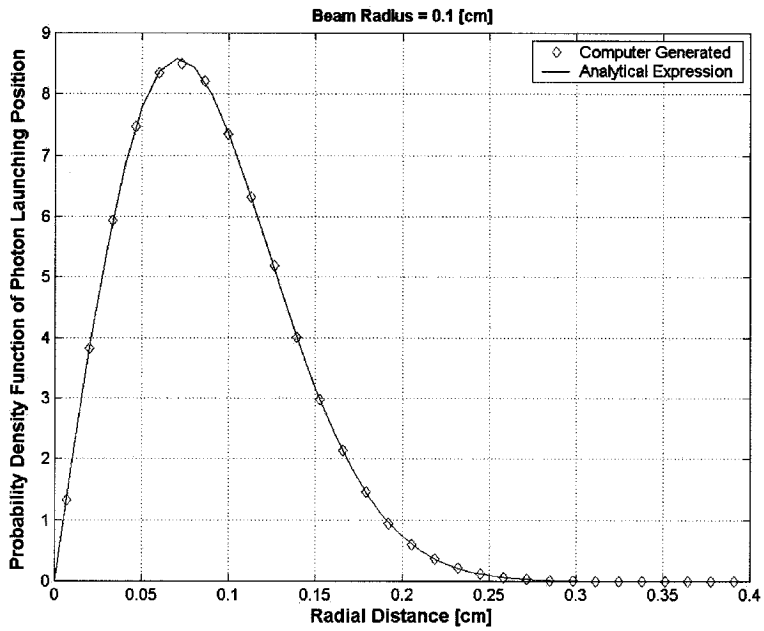

Figure (3-5) Probability density function of photon radial launching position of a Gaussian beam profile with $1/e^2$ radius of 0.1 cm according to sampling rule II.

The computer generated probability density function was constructed according to equation (3-16) using the normalized histogram of the random variable r_1. One million randomly generated numbers (ξ_1) were used for this purpose. A graphical comparison between figures (3-3) and (3-5) reveals differences in the width and the height of the two probability density functions. Although the plot of the normalized intensity as suggested by equation (3-16) shows a Gaussian profile as seen in figure (3-6), there is a noticeable

difference between the width and the height of the two intensities in figures (3-4) and (3-6).

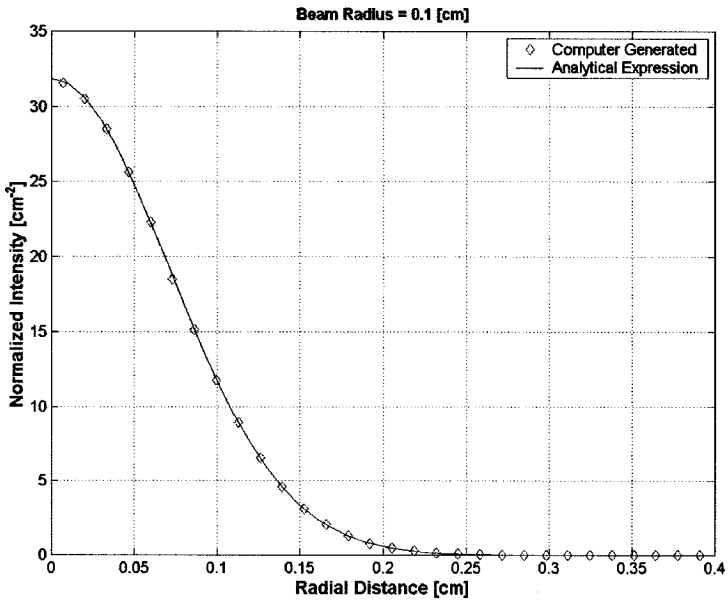

Figure (3-6) Normalized intensity profile according to sampling rule II.

It can be noticed by comparing figures (3-4) and (3-6) that, the intensity value drops to $1/e^2$ of its maximum at the beam radius of 0.1 cm, as seen in figure (3-4). The intensity profile depicted in figure (3-6) does not show a similar characterizing feature. However, at 0.1 cm the beam intensity approximately drops to 1/e of its maximum value as if figure (3-6) represents the Electric field of the Gaussian beam and not the intensity. As mentioned before, Monte Carlo method can simulate energy distribution profile within a turbid medium but it does not model electric fields within the medium. This is an indication that sampling rule II, suggested by equation (3-16), is inaccurate in representing a Gaussian beam profile in Monte Carlo simulation. In the coming chapter, verification of the accuracy of sampling rules I&II is further investigated by means of Monte Carlo Simulation.

3.3 Monte Carlo Photon Launching Algorithm in the Focused Gaussian Beam Model

So far, only collimated optical beams, which are normally incident on multi-layered tissue, have been discussed. However, in many applications of laser in biophotonics it is necessary to produce a smaller spot size by means of focusing lenses. As mentioned in the previous chapter in section (2.3.2), it is assumed that in modeling a focused Gaussian beam, the depth of focus of the incident beam is much longer than the focal length f of the focusing lens. Therefore, the transmitted beam is focused at the lens' focal plane as would be expected for parallel rays incident on the lens. The geometric-focus method was adapted to model focusing of the beam with Monte Carlo simulation. In this method, the initial position of the photon to be launched is determined stochastically according to the intensity profile of the incident beam (uniform or Gaussian). Once the initial position of the photon has been chosen according to the desired probability distribution function, the photon is directed towards the geometric focus of the beam [6,31-35]. The initial coordinates of the photon and its launching directional cosines govern the behavior of the laser beam propagating through the medium in the absence of scattering. Therefore, one can study the effect of scattering medium on a propagating laser beam by determining the distortion resulting from the scattering properties of this medium.

As mentioned before, the MCML program can only calculate the impulse response of an infinitely narrow photon beam incident perpendicularly on multi-layered tissue. The CONV program processes the output of the MCML program to calculate the response due to an incident finite diameter collimated photon beam. The CONV program basically uses numerical integration methods to convolve the impulse response of the incident infinitely narrow beam calculated by the MCML program. Therefore, It was necessary to

modify the MCML source code to allow for the modeling of a finite diameter optical beam, with the desired intensity profile, to be modeled under different focusing conditions.

The Monte Carlo modeling method was applied previously to model focusing of light beams into optically turbid tissue for several purposes. For example, the study of the performance of imaging techniques used in diagnosis such as Optical Coherence Tomography [31,32,34,36,37], confocal microscopy [35,38,39], and two photon excitation microscopy [40,41]. Absorbed optical power in Photodynamic therapy [33] and the optical distribution within turbid media in general [6,33] were also studied. Figure (3-7) shows the geometry of the focusing optical beams into a homogeneous turbid medium according to the geometric-focus method.

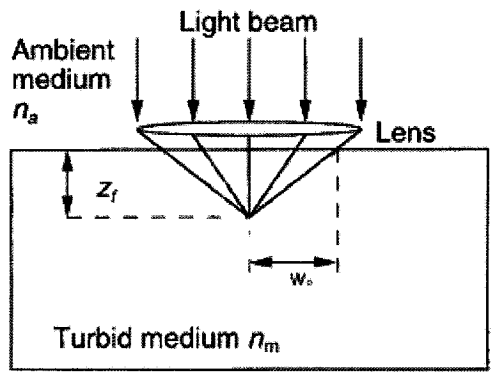

Figure (3-7) Schematic of the focusing model geometry

For tracing the photons that are launched into the medium, a Cartesian coordinate system was used. The center of the coordinate system was taken to be the center of the incident beam. The x-y plane is the surface of the turbid medium and the z-axis is pointing towards the inside of the medium. Equation (3-14) determines the radial launching position of photons within a Gaussian beam profile of $1/e^2$ radius of W_o, and equation (3-

5) is used to sample the radial angle Φ. The Cartesian coordinates of the incident photons are determined according to equations (3-6) and (3-7):

If Z_f is the depth of the focal point of the used lens in the turbid medium, then the directional cosines of the launched photons in the medium are given by:

$$u_x = \frac{-x}{\sqrt{r_l^2 + Z_f^2}} \tag{3-17}$$

$$u_y = \frac{-y}{\sqrt{r_l^2 + Z_f^2}} \tag{3-18}$$

$$u_z = \frac{z_f}{\sqrt{r_l^2 + Z_f^2}} \tag{3-19}$$

In order to obtain an acceptable statistical variance for the recorded light absorption, reflection and transmission, a large number of photons had to be traced in the tissue. In this study, two million photons were traced [6]. In this model, the refractive index of the ambient medium is matched with the refractive index of the turbid medium. This assumption will help in avoiding the implementation of Snell's law at the boundary between the ambient and tissue, which leads to focusing distortion. In the next chapter, the Monte Carlo simulation results of the above-described model are presented.

3.4 Summary

In this chapter, a Monte Carlo Model for a focused Gaussian beam was presented. This model will be applied to multi-layered tissue structures in the coming chapters. The Monte Carlo sampling rules of both uniform intensity and Gaussian beams were derived in detail. A proposed sampling rule of a Gaussian beam profile was compared analytically with another sampling rule used in the literature [31,32]. The focusing method of photons using the geometric-focus method and how to realize the focusing method in Monte Carlo simulation was also covered.

CHAPTER 4

Verification of the Monte Carlo Model by Simulation

4.0 Introduction

This chapter presents the simulation results of the Monte Carlo model for a focused optical beam into multi-layered tissue in general. It is concerned with verification of the model by means of comparing its results with published reports. The comparison between the output of our Monte Carlo simulation model with the output of the MCML and CONV programs [25,27] was done for the case of collimated incident Gaussian beam. The case of a multi-layered tissue in references [26,27] was taken to be the basis for the comparison. The newly proposed equation for sampling the Gaussian beam profile (sampling rule I) is compared with the one mentioned in references [31,32] (sampling rule II). The inaccuracy of the sampling rule II, given by equation (3-16), which was discussed analytically in the previous chapter, is proved by simulation in this chapter. For verifying the focusing method adapted in our model, a comparison between a published model for focusing uniform intensity light into a homogeneous turbid medium [6] with

our model was done. For the sake of comparison, our model was set to simulate a uniform intensity laser beams under different focusing conditions according to reference [6].

4.1 Simulation Results of Multi-Layered Tissue

The verification of our model will start by comparing the impulse responses of a multi-layered tissue as calculated by the MCML program and our program. By setting the radius of the incident beam in our model to an extremely small value, the condition of an infinitely narrow photon beam can be realized. The second stage of the verification process involves the comparison between the responses of the multi-layered tissue due to a collimated, finite diameter beam normally incident on the tissue. In this stage an incident collimated Gaussian beam of total energy 1 Joule, and $1/e^2$ beam radius of 0.1 cm is used. These values specifying the Gaussian beam were used in references [26,27]. The optical properties of the three layers are summarized in a table form for simplicity of comparison. In this study, the grid separation in both the z and r directions is 0.01 cm and the number of grid elements in the z direction is 40 and in the r direction is 50.

Table (4-1) Optical Properties of the three-layer tissue. Top and bottom ambient media refractive indices were taken as unity [26,27]

Layer	Refractive index (n)	Absorption coefficient. μ_a cm^{-1}	Scattering Coefficient. μ_s cm^{-1}	Anisotropy factor g	Thickness cm
1	1.37	1	100	0.9	0.1
2	1.37	1	10	0	0.1
3	1.37	2	10	0.7	0.2

In this simulation, the refractive index of the ambient medium right above and right below the three layers is taken to be 1. References [26,27] used one million photons for this study and therefore the same number of photons was used in our model as well.

Since the CONV program uses an extended trapezoidal rule to perform the numerical integration, the convolution error used in the CONV program was set to 0.001. Since the numerical integration carried by the CONV is computed iteratively, the iteration is controlled by the amount of the error between the new estimated value and the old estimated value. If the error value in the CONV program was chosen to be larger than necessary, the precision of the calculation will deteriorate and the resulting convolved values may suffer from discontinuities. Smaller values of integration error will lead to high precision results but consumes more time to be done. Typically the allowed range of the integration error in the CONV program lies within the limits of 0.001 to 0.1. The simulation output provides calculations of three physical quantities of interest: the radially resolved diffuse reflectance in J/cm^2, the radially resolved total transmittance in J/cm^2, and the fluence in J/cm^2 at different depths from the surface of the examined tissue. We need to mention that; both MCML and CONV programs produce simulation results as ASCII output arrays. The results then are plotted using any suitable commercial plotting software.

4.1.1 Impulse Responses of the Three-Layer Tissue Model

The first step in the model verification process is to insure that the developed simulation program produces the same impulse response to an infinitely narrow, normally incident photon beam as the original MCML simulation program. In our model, an arbitrarily small beam radius was selected (1E-08 cm) to simulate an infinitely narrow photon beam. Following are the obtained results from the simulation runs.

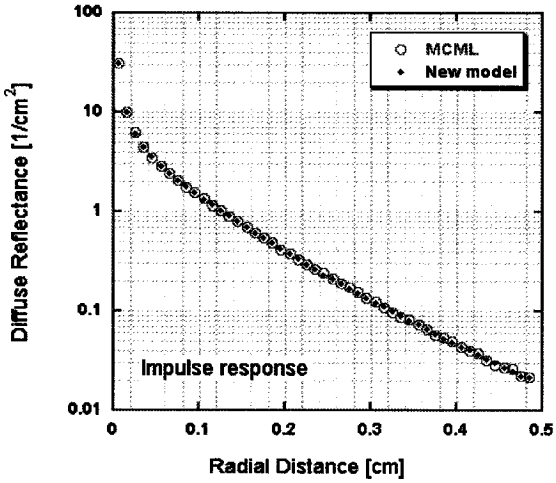

Figure (4-1) Radially resolved diffuse reflectance due to an infinitely narrow, normally incident photon beam.

Figure (4-1) shows the comparison between the radially resolved diffuse reflectance as calculated by the two simulation programs. As the legend above the graph indicates, "MCML" stands for the simulation results as calculated by the original MCML code released by Wang *et al.* [25]. The MCML code simulates only infinitely narrow photon beams, normally incident on the multi-layered tissue. The new model of a finite diameter focused optical beam into multi-layered tissue was fed by an arbitrarily small incident beam radius (1E-08 cm) to simulate the infinitely narrow beam radius. An infinite depth of focal point in the tissue (1E+08 cm), which is equivalent to "no focusing" or collimated incident photon beam, was also input to the model (refer to figure (3-7) for model geometry). A total number of one million photons were used in this simulation. The obtained results of the new model come to an excellent agreement with the results of the original MCML program as it can be seen in figure (4-1). Figure (4-2) shows the radially resolved total transmittance in cm^{-2} due to an infinitely narrow, normally incident photon beam. This result shows an excellent match with the calculated impulse response of the original MCML program.

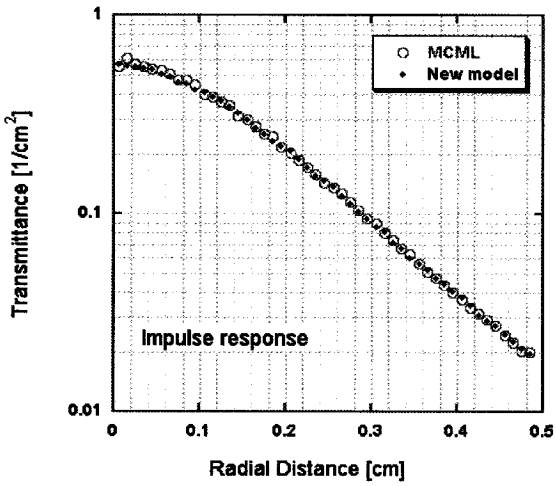

Figure (4-2): Radially resolved total transmittance due to an infinitely narrow, normally incident photon beam.

Figures (4-3), (4-4) show the fluence in cm^{-2}. The fluence rate is a very important quantity in the field of laser dosimetry. The formal definition of radiant energy fluence rate (Watt cm^{-2}) is: "at a given point in space, the radiant energy flux incident on a small sphere, divided by the cross sectional area of that sphere" (ISO 31/6, 1980). If the total optical absorption coefficient at a given wavelength is μ_a in cm^{-1}, the fluence rate is the absorbed power divided by μ_a. It should be clear that the fluence (J cm^{-2}) is the time integral of the fluence rate [42]. The MCML program records photon deposition in cm^{-3} due to absorption in each grid element of a spatial array, and finally calculates fluence, in cm^{-2} by dividing deposition by the local absorption coefficient, μ_a in cm^{-1}. The calculated fluence from the two programs comes to a perfect match as shown in figures (4-3) and (4-4). We need to mention that the spatial grid system in the radial direction r was limited to 0.5 cm in the original study [26,27]. This is the reason behind limiting the radial grid system to the same value in our study.

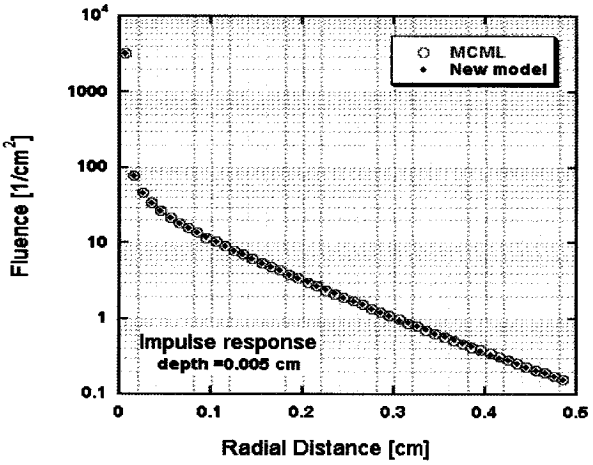

Figure (4-3) Radially resolved total fluence at a depth of 0.005 cm due to an infinitely narrow, normally incident photon beam.

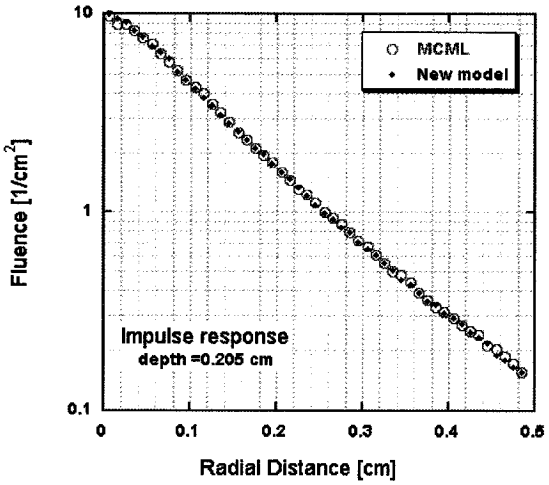

Figure (4-4) Radially resolved fluence at a depth of 0.205 cm due to an infinitely narrow, normally incident photon beam.

4.1.2 Responses of the Three-Layer Tissue due to a Normally Incident Finite Size Collimated Gaussian Beam

In this section the obtained results from the simulation runs of a collimated Gaussian photon beam incident on the three-layered tissue under study are presented. The intensity profile at a transverse plane to the direction of propagation theoretically extends to infinity. However, at the defined $1/e^2$ Gaussian beam radius, the intensity drops to about

0.135 of its peak value at the beam center and hence, about 86% of the beam power is contained within this radius [30]. This is the philosophy behind using the term "finite size" when describing the Gaussian beam. It should be noted that the launching of the Monte Carlo photons obeys the Monte Carlo sampling rule described by equation (3-14), and discussed in the previous chapter, and is not limited to radial positions that are within the $1/e^2$ beam radius. The term "collimated", which refers to beams with planar wave fronts, can be used to describe a Gaussian beam at the transverse plane containing the beam waist. In our model, it is assumed that the Gaussian photon beam hits the surface of the tissue with a beam radius equal to the waist radius. The optical properties of the layers are cited in table (4-1), and the incident beam parameters are 0.1 cm beam radius and total energy of 1 Joule. The results of our model are compared with the results calculated by the MCML program and further processed by the associated CONV program. The simulation results of a finite size collimated Gaussian beam based on the Monte Carlo sampling rule suggested by references [31,32] are also presented in this section and compared with the other results. The calculated physical quantities by Monte Carlo simulation according to equation (3-14), proposed in this thesis, will be denoted as "Sampling rule I". On the other hand, those quantities, which are calculated according to equation (3-16), and proposed in [31,32], will be denoted as "Sampling rule II".

4.1.2.1 Radially Resolved Diffuse Reflectance of the Three-Layer Tissue

The results in this section are presented for two different Gaussian beam radii of 0.1 and 0.2 cm respectively. The second beam radius of 0.2 cm is arbitrarily selected to represent the case of increasing the beam radius in comparison with the published responses at the radius of 0.1 cm. The change in the incident beam radius will help in discovering the

relation between changing the beam size and sampling rules I&II. Changing the incident beam radius will also help in verifying the newly developed simulation program and test its validity at different input beam radii. Figure (4-5) shows the radially resolved diffuse reflectance due to a normally incident, collimated Gaussian photon beam with total energy of 1 Joule and beam radius of 0.1 cm. The legend " MCML-CONV" refers to the calculated response by the MCML program that was further processed by the CONV program to yield the final response due to a finite size Gaussian beam that is normally incident of the tissue.

Figure (4-5) shows excellent match between the results obtained by using the proposed sampling rule I and the results cited in references [25-27]. We notice that CONV program underestimates the value of the diffuse reflectance near the end of the radial grid elements as shown. Due to the spatially limited grid system, the integration evaluated by the CONV program may suffer from clipping of its upper integration limit [26]. This causes the CONV program to underestimate the true value of the integration as the last grid element is approached. This can explain the drop of the value of the diffuse reflectance of the CONV program as we approach the maximum of the grid system at $r = 0.5$ cm in this simulation run.

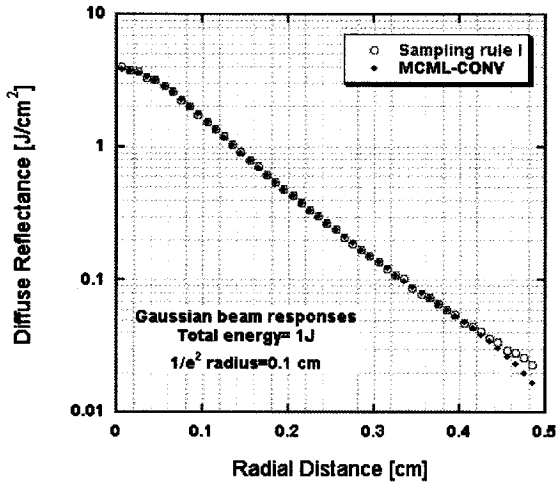

Figure (4-5) Radially resolved diffuse reflectance due to a normally incident collimated Gaussian photon beam of radius= 0.1 cm, and Gaussian sampling rule I

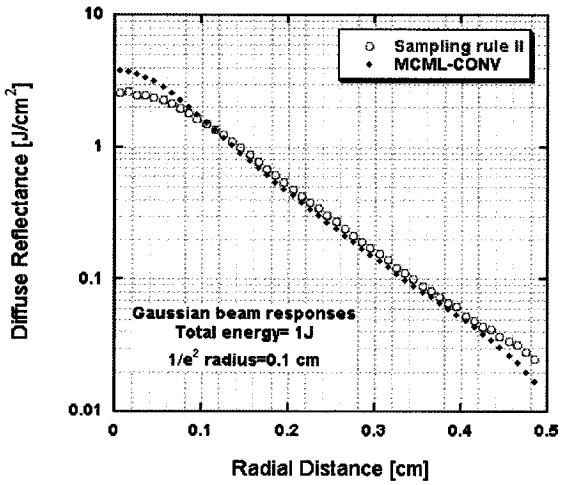

Figure (4-6) Radially resolved diffuse reflectance due to a normally incident collimated Gaussian photon beam of radius=0.1 cm, and Gaussian Sampling rule II

Figure (4-6) shows the diffuse reflectance due to a normally incident collimated Gaussian photon beam and Gaussian sampling rule II, compared with the output of the MCML and CONV programs. The difference between the two results is noticeable especially within the radial distance that is approximately equal to the beam radius (0.1 cm). The deviation in the obtained results starts with a maximum at the beam center (radial distance = 0), when using sampling rule II compared with the reference output of the CONV program, and then decreases gradually until the two results match at a radial distance

approximately equal to the beam radius. After the intersection between the two curves, the difference in the results starts to increase again but in the opposite direction. In other words, from the beam center to the beam radius, the sampling rule II underestimates the true value of the measured quantity (diffuse reflectance). After a radial distance equal to the beam radius, sampling rule II overestimates the value of the measured quantity. It is important to notice that the calculated diffuse reflectance at the beam center is approximately 3.9 cm^{-2} as calculated by the CONV program while diffuse reflectance at the same point is evaluated to be 2.6 cm^{-2} by the simulation program if it adapts the Gaussian sampling rule II. This represents an error of approximately 33%. For applications where the measurement of the diffuse reflectance is required, the above-mentioned Gaussian sampling rule II represents a source of considerable error. Figure (4-7) shows the comparison between radially resolved diffuse reflectances due to a normally incident collimated Gaussian photon beam of radius 0.1 cm, based on sampling rules I&II.

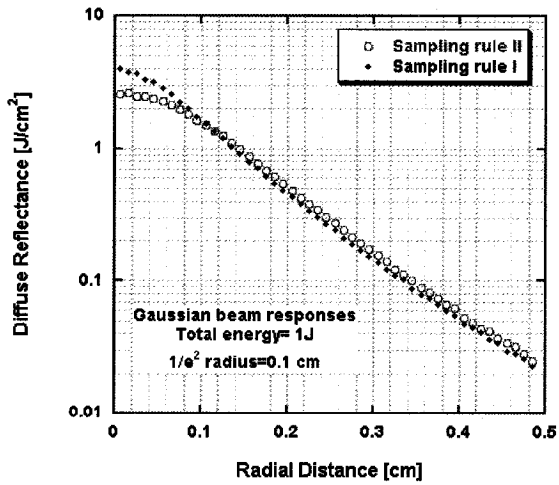

Figure (4-7) Comparison between radially resolved diffuse reflectances due to a normally incident collimated Gaussian photon beam of radius =0.1 cm, according to the Gaussian sampling rules I&II

The simulation results of diffuse reflectance due to a normally incident collimated Gaussian photon beam of radius 0.2 cm are presented next. Figure (4-8) shows the excellent match in results between the suggested sampling rule I, and the reference results obtained from the CONV Program.

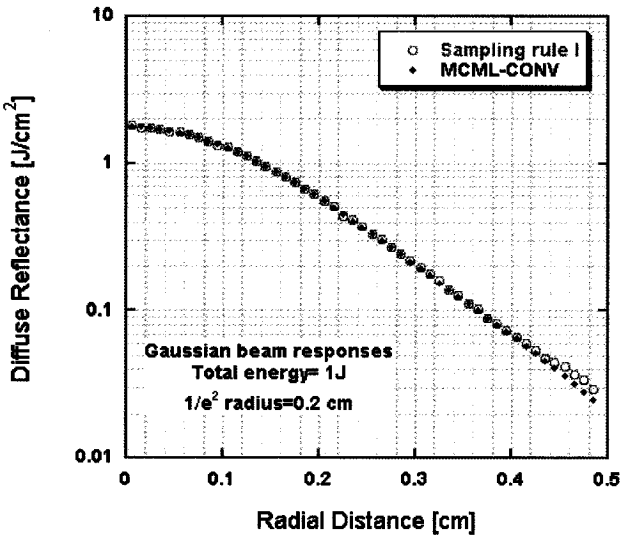

Figure (4-8) Radially resolved diffuse reflectance due to a normally incident collimated Gaussian photon beam of radius= 0.2 cm, and Gaussian sampling rule I

Figure (4-9) shows the error in calculating the diffuse reflectance using the Gaussian sampling rule II suggested in references [31,32]. The error in calculating the diffuse reflectance near the beam center approaches 36%, which is unacceptable error. The same behavior of the intersecting curves around a radial distance approximately equal to the beam radius (0.2 cm) is noticed. Overestimation of the true value of the diffuse reflectance at radial distances greater than the beam radius is noticed. Underestimation of the true value of reflectance is recorded at radial distances less than the beam radius. This behavior of the error has become clearer as the beam radius was increased from 0.1 cm to 0.2 cm.

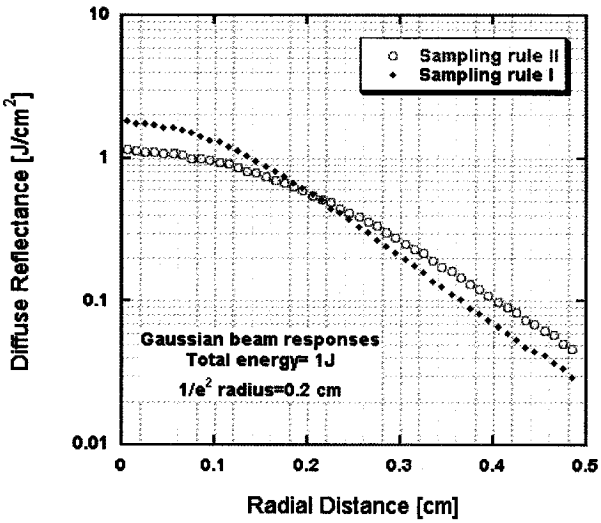

Figure (4-9) Comparison between radially resolved diffuse reflectances due to a normally incident collimated Gaussian photon beam of radius =0.2 cm, according to Gaussian sampling rules I&II.

4.1.2.2 Radially Resolved Total Transmittance of the Three-Layer Tissue

The radially resolved total transmittance simulation results are shown in this section in figures (4-10) to (4-13). The case of an incident beam with radius 0.1 cm is shown in figures (4-10) and (4-11). It is noticed from figure (4-11) that the error in the calculation of the total transmittance according to the Gaussian sampling rule II is not large due to the fact that the intensity of the transmitted portion of light is very weak (The maximum transmittance in the figure is in the order of 0.5 cm^{-2}). This behavior may be explained in light of the fact that the suggested Gaussian sampling rule I is directly dependent on the intensity profile of the Gaussian beam while sampling rule II can not be considered as an accurate representation of the Gaussian intensity profile as explained in section (3.2). However, at low intensities sampling rules I&II converge in their behavior. Therefore, the physical quantities with low intensities recorded in the grid system deviate less from the standard response if sampling rule II is used. Figures (4-13) and (4-14) show the

simulated radially resolved total transmittance due to a normally incident collimated Gaussian photon beam of radius= 0.2 cm, and Gaussian sampling rules I&II.

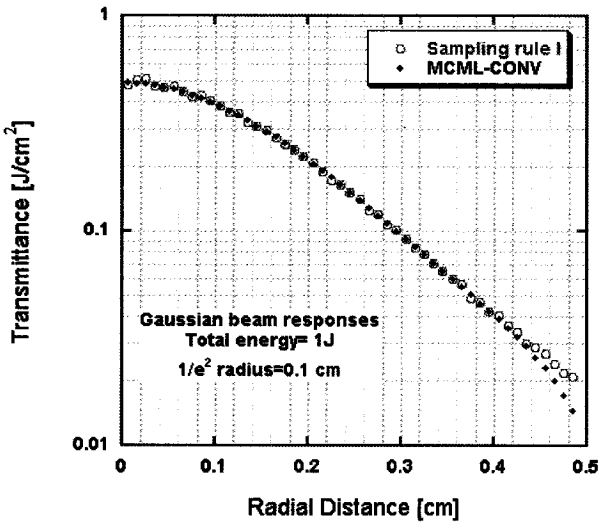

Figure (4-10) Radially resolved total transmittance due a normally incident collimated Gaussian photon beam of radius=0.1 cm, and Gaussian sampling rule I

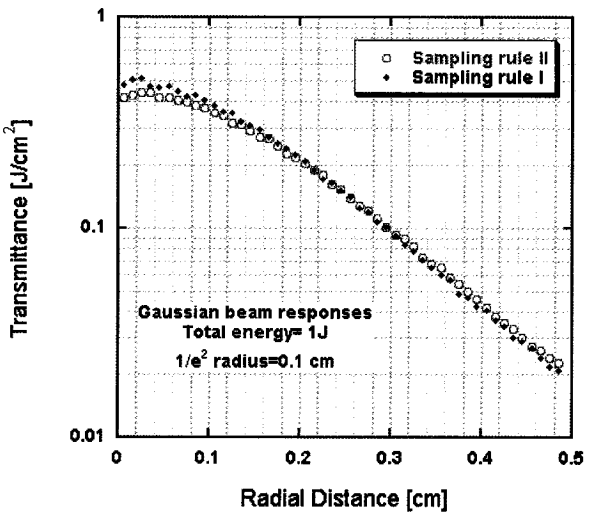

Figure (4-11) Comparison between radially resolved total transmittance due to a normally incident collimated Gaussian photon beam of radius =0.1 cm, according to Gaussian sampling rules I&II

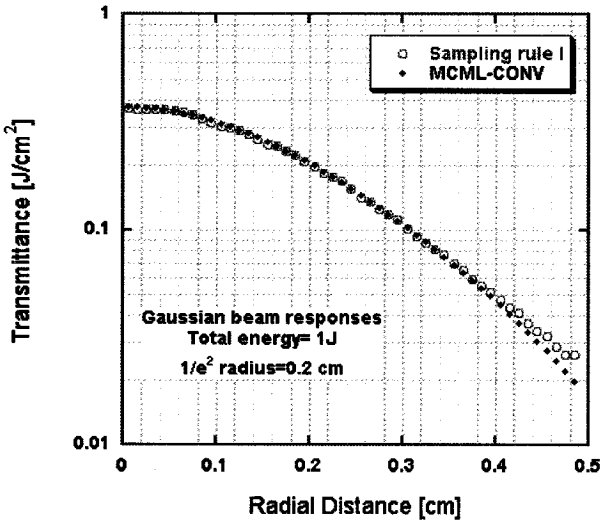

Figure (4-12) Radially resolved total transmittance due to a normally incident collimated Gaussian photon beam of radius=0.2 cm, and Gaussian sampling rule I

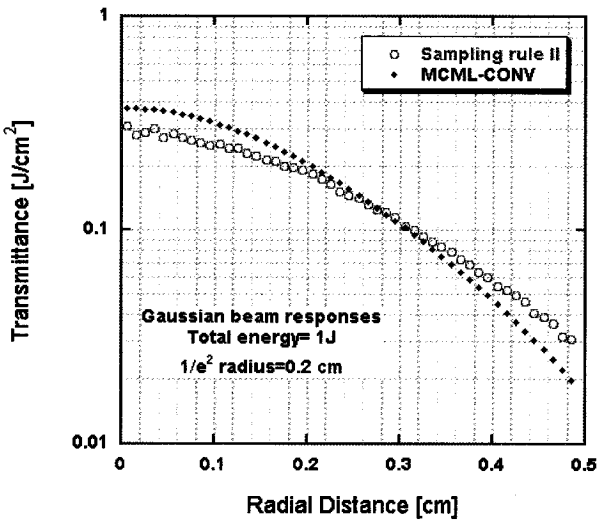

Figure (4-13) Radially resolved total transmittance due to a normally incident collimated Gaussian photon beam of radius= 0.2 cm, and Gaussian sampling rule II

4.1.2.3.Radially Resolved Fluence of the Three-Layer Tissue at Depths of 0.005 and 0.205 cm

The radially resolved fluence calculated at these two specific depth planes were chosen by Wang and Jacques [26,27] to verify the CONV program. This is the reason for the choice of these specific values of depth to calculate the fluence. Figure (4-14) shows an

excellent match between the calculated fluence by our model (based on sampling rule I) and the results obtained by references [25-27]. Figure (4-15) shows a considerable error in the calculation of fluence between the model based on sampling rule II and references [25-27].

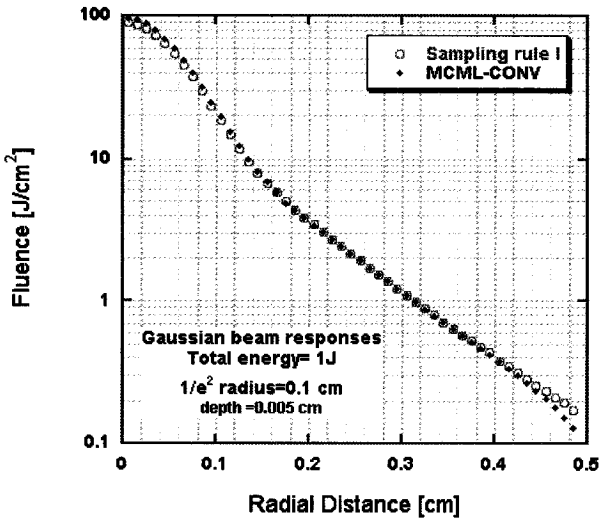

Figure (4-14) Radially resolved fluence at a depth of 0.005 cm due to a normally incident collimated Gaussian photon beam of radius =0.1 cm, and Gaussian sampling rule I

The error in the calculation of the fluence near the center of the beam as calculated from figure (4-15) is approximately 48%. This means that, the simulation of the fluence based on sampling rule II and suggested in references [31,32], can cause an underestimation of the actual fluence by almost 50% near the center of the beam. The comparison between the Gaussian sampling rules I&II in figure (4-16) shows a considerable difference between the two results.

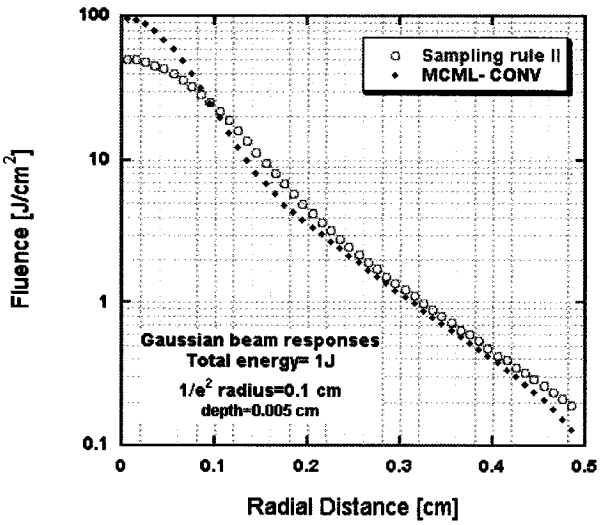

Figure (4-15) Radially resolved fluence at a depth of 0.005 cm due to a normally incident collimated Gaussian photon beam of radius =0.1 cm, and Gaussian sampling rule II

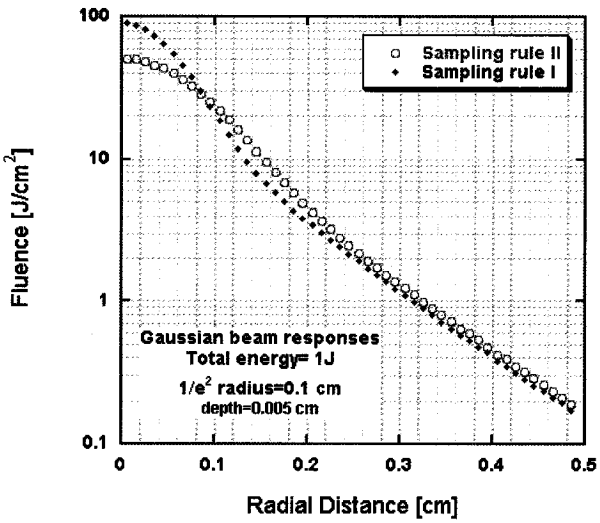

Figure (4-16) Comparison between radially resolved fluences at a depth of 0.005 cm due to a normally incident collimated Gaussian photon beam of radius =0.1 cm, and Gaussian sampling rules I&II

The fluence results at a larger depth in the tissue under study were also simulated. The second depth of interest was taken at 0.205 cm below the surface of the three-layer tissue described in table (4-1). As mentioned before, this specific value of the depth in tissue was chosen by reference [26] and therefore is chosen here for making comparison with

the same reference. Figure (4-17) shows the result of calculating the fluence at a depth of 0.205 cm in the tissue based on sampling rule I. The agreement between our model and references [25-27] is clear from the figure below. The deviation between the two results at radial distances close to the last grid element is due to the spatial limitation of the grid system as it was explained for figure (4-5).

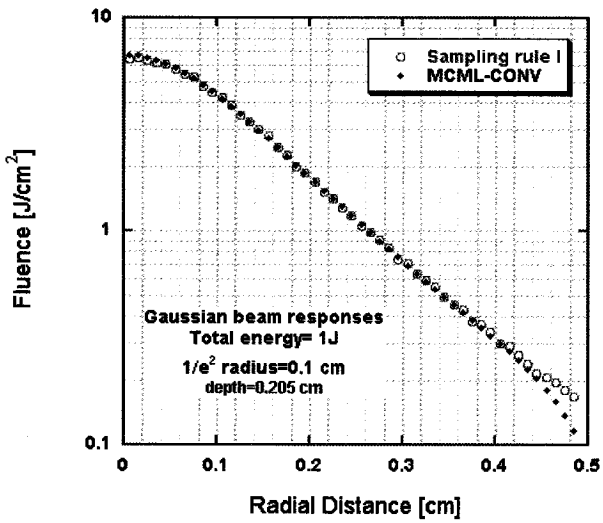

Figure (4-17) Radially resolved fluence at a depth of 0.205 cm due to a normally incident collimated Gaussian photon beam of radius =0.1 cm, and Gaussian sampling rule I

Figure (4-18) shows the radially resolved fluence at a depth of 0.205 cm due to a normally incident collimated Gaussian photon beam of radius =0.1 cm, and Gaussian sampling rule II. It is clearly noticed from this figure that the error in evaluating the actual fluence near the beam center is about 17%. Comparing this error to the error at the same radial position, but at a depth of 0.005 cm from the tissue surface according to figure (4-15) is about 48%.

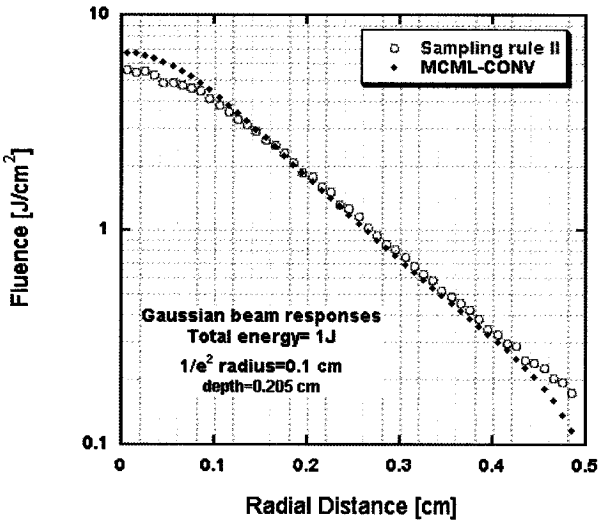

Figure (4-18) Radially resolved fluence at a depth of 0.205 cm due to a normally incident collimated Gaussian photon beam of radius =0.1 cm, and Gaussian sampling rule II

It is noticed that, as the scored physical quantity has a higher intensity, the error associated with the Gaussian sampling rule II described by equation (3-16) increases and vise versa.

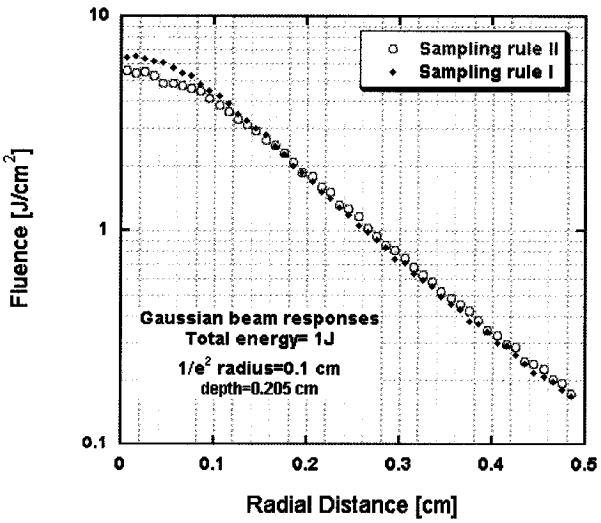

Figure (4-19) Comparison between radially resolved fluences at a depth of 0.205 cm due to a normally incident collimated Gaussian photon beam of radius =0.1 cm, and Gaussian sampling rules I&II

The effect of increasing the beam radius from the case of 0.1 cm to an arbitrarily selected larger beam radius of 0.2 cm on the calculated fluences at the same different depths from tissue surface is shown in figures (4-20) to (4-23).

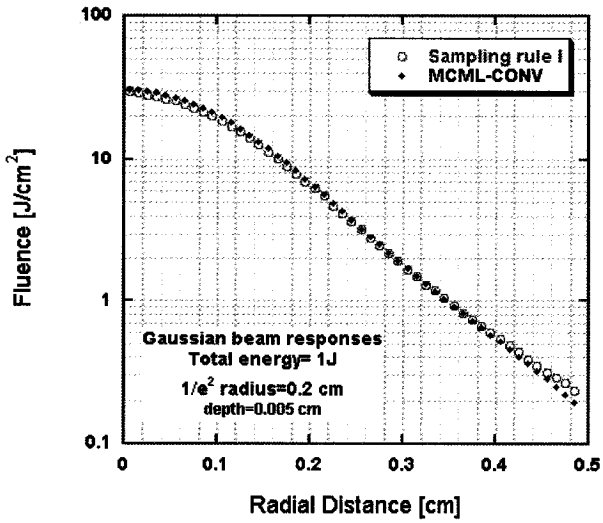

Figure (4-20) Radially resolved fluence at a depth of 0.005 cm due to a normally incident collimated Gaussian photon beam of radius =0.2 cm, and Gaussian sampling rule I

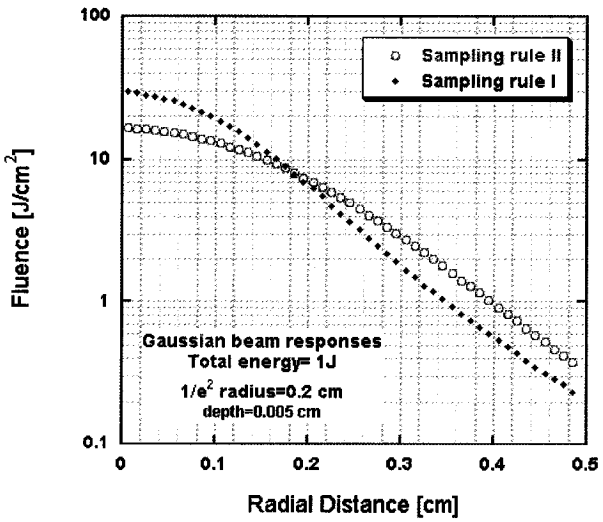

Figure (4-21) Comparison between radially resolved fluences at a depth of 0.005 cm due to a normally incident collimated Gaussian photon beam of radius =0.2 cm, and Gaussian sampling rules I&II

Based on sampling rule I, the calculated fluence by our model matched the results of references [25-27] at the new beam radius. The increase in the incident beam size did not cause a noticeable error of the calculated fluence at the two depths of 0.005 and 0.205 cm as shown in figures (4-20) and (4-22). The deviation of the obtained results from those of references [25-27] as the last grid element in the grid system is approached, is due to the spatial limitation of the grid system, which causes the CONV program to underestimate the true value of integration representing the physical quantity calculated [26,27]. When sampling rule II is applied to our model, the calculated results of the fluence at the two different depths of interest, deviate considerably from the results presented by references [25-27] as seen in figures (4-21) and (4-23). The error in the estimation of the fluence near the beam center is approximately 46% as it can be seen from figure (4-21).

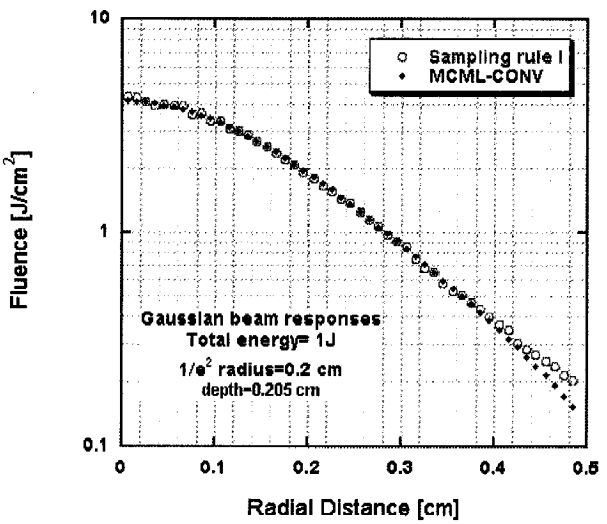

Figure (4-22) Radially resolved fluence at a depth of 0.205 cm due to a normally incident collimated Gaussian photon beam of radius =0.2 cm, and Gaussian sampling rule I

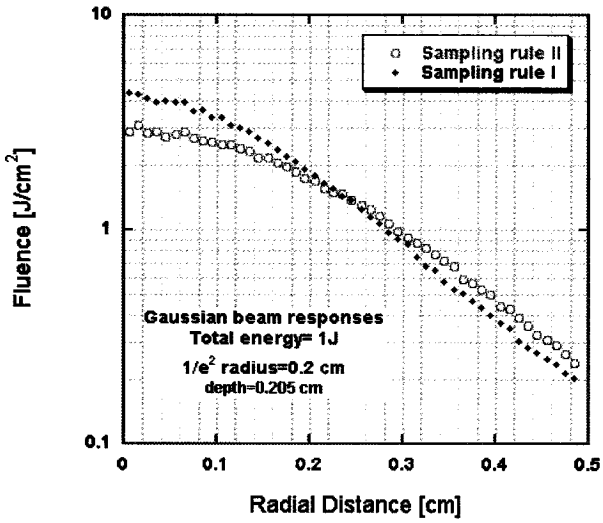

Figure (4-23) Comparison between radially resolved fluences at a depth of 0.205 cm due to a normally incident collimated Gaussian photon beam of radius =0.2 cm, and Gaussian sampling rules I&II

4.2 Simulation Results of the Absorption Distribution of a Focused Uniform Intensity Optical Beam into a Homogeneous Turbid Medium.

In this section the results of the Monte Carlo simulation model of a focused optical beam into a homogeneous turbid medium are presented. The importance of these simulation results for our Monte Carlo model can be summarized in two points. First, it provides double verification to our Monte Carlo simulation program developed to simulate the focusing of optical beams into multi-layered tissue. Comparing the results obtained by our Monte Carlo simulation program with the published results obtained by Wang and Liang [6], using another Monte Carlo simulation program, the verification of the focusing method can be achieved as the verification of the sampling method was already done in the previous section. Second, the cases of focusing an optical Gaussian beam into a homogeneous turbid medium and into a human skin model are explored. The study carried out by Wang and Liang considered only the case of a uniform intensity optical

beam focused into a homogeneous turbid medium. In many applications of Laser therapy, the knowledge of the absorption distribution within the tissue under study is of top importance. The delivery of the Laser beam is usually done by means of a focusing lens in order to increase the absorption peak within the medium.

Wang and Liang [6] studied the distribution of an optical beam focused into a turbid medium by Monte Carlo simulation technique. In that study, a model of an infinite homogeneous medium was considered among other models. For the model under investigation, the optical properties of the medium where taken as follows: refractive index of the medium n_m= 1.4, absorption coefficient μ_a= 0.1 cm^{-1}, scattering coefficient μ_s= 100 cm^{-1} and the anisotropy factor g = 0.9. The ambient surrounding the sample medium has a matched index of refraction to that of the turbid medium (ambient refractive index n_a=1.4). The matched indices between the turbid medium and the ambient will help in excluding the effect of aberration in which different rays converge to different points instead of one point in the imaging plane. This is to say, mismatched indices will impose Snell's law at the boundary at the ambient tissue interface, which will cause focusing distortion. It is required to study the absorption distribution of light affected only by the scattering properties of the medium, excluding any other factors. Therefore, the simplification of matching the ambient-tissue interface is relevant to the case study. The sizes of the grid elements for the Monte Carlo simulations in the *x*, *y*, and *z* directions were 0.05, 0.05, and 0.025 cm, respectively. Table (2-4) summarizes the optical properties of the homogeneous turbid medium under study.

Table (4-2) Optical properties of the infinite homogeneous turbid medium under study. Top and bottom ambient media refractive indices were taken as n_a= 1.4

Layer	Refractive index (n)	Absorption coefficient. μ_a cm^{-1}	Scattering Coefficient. μ_s cm^{-1}	Anisotropy factor g	Thickness cm
1	1.4	0.1	100	0.9	∞

In the following sections the simulation results of absorption distribution of a uniform intensity focused beam into a homogeneous turbid medium are presented and compared with the published results by Wang and Liang [6]. It needs to be mentioned here that, the tracing of Monte Carlo photons in the study carried out in reference [6] was based on the delta scattering technique [23], while our photon tracing method is based on the variance reduction technique which is the standard Monte Carlo method for photon tracing [25,26]. The geometry of Monte Carlo model for focusing optical beams into homogeneous turbid medium is shown in figure (3-7), but is repeated here for convenience as figure (4-24). The approach of geometric-focus method for focusing photons is adapted in this model. As mentioned before, the geometric-focus method involves the selection of the initial position of the photon to be launched stochastically according to the beam intensity profile. The selected photon packet is then directed to the geometric focus of the beam.

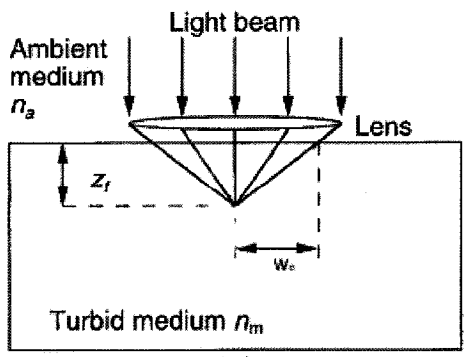

Figure (4-24) Schematic of the focusing model geometry

Figure (4-24) shows the geometry of the model of a focused optical beam into a homogeneous turbid medium. Z_f in this figure is the depth of the focal point in the turbid medium. Z_f will be changed during the simulation in order to study the effect of focusing on the absorption distribution inside the turbid medium. An incident optical beam of radius 0.5 cm is focused into the medium. Figure (4-25) shows the simulation results of the absorption distribution of a uniform intensity focused beam into a homogeneous turbid medium under different focusing conditions. The depth of the focal point Z_f was set to 0.05 cm, 0.1 cm, 0.2 cm and ∞. (∞ is equivalent to a collimated beam). In order to study this model by Monte Carlo simulation two million photons in each simulation run were used to ensure an acceptable reduced variance in the calculated results. This number of photons is within the number of photons range that is recommended in [6]. From figure (4-25) below we can see that the focusing process greatly affects the absorption distribution of the optical beam in the homogeneous turbid medium.

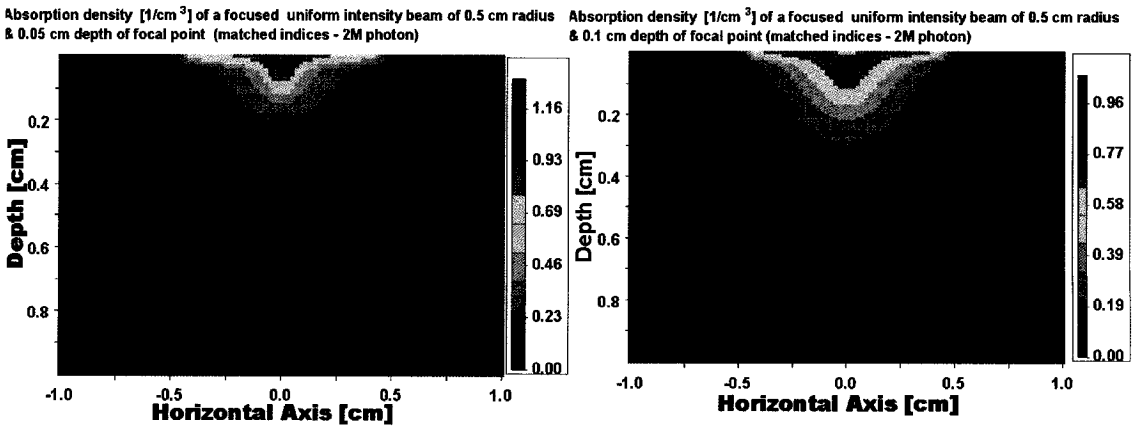

(a) (b)

Figure (4-25) Absorption distribution of a uniform intensity focused optical beam in a homogeneous turbid medium under different focusing conditions. (a) Depth of focal point Z_f= 0.05 cm. (b) Depth of focal point Z_f = 0.1 cm.

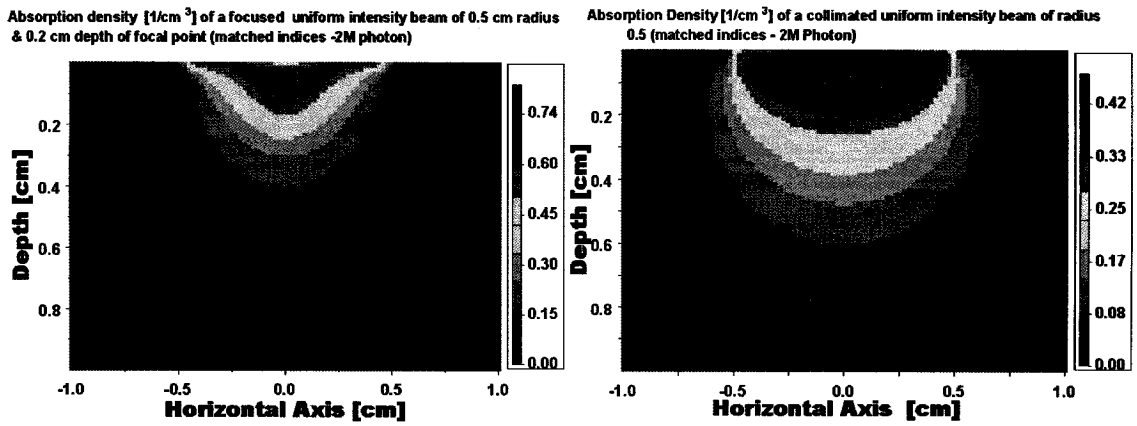

(c) (d)

Figure (4-25) Absorption distribution of a uniform intensity focused optical beam in a homogeneous turbid medium under different focusing conditions (c) Depth of focal point $Z_f = 0.2$ cm. (d) Depth of the focal point $Z_f = \infty$ cm. In all cases the radius of the incident optical beam before focusing is 0.5 cm and two million photons are launched in each simulation run.

As the depth of the focal point is very small and close to the medium surface, a peak in the absorption density as well as a confinement in the absorption profile are noticed. As the depth of the focal point increases towards infinity (collimated beam), the peak absorption density decreases and the absorption profile loses its confinement. Therefore, the effect of focusing loses its main features regarding the increase in the peak absorption and the confinement of the absorption profile at large depths from the tissue surface. The factor that is used in determining the depth of the focal point after which the focusing process would be inefficient is the transport mean free path [6]. The transport mean free path is defined as $[\mu_a+\mu_s(1-g)]^{-1}$. In our case, the transport mean free path is equal to 0.099 cm. The effect of focusing, after the depth of focal point is larger than 0.1 cm, starts to be inefficient. It is worth mentioning that because of the optical properties of the medium under study, there will be neither transmittance nor specular reflectance to calculate. Figure (4-26) shows the absorption distribution of a uniform intensity focused optical beam in a homogeneous turbid medium under different focusing conditions

obtained by Wang and Liang [6]. Comparing these results with the results in figure (4-25), good agreement is noticed.

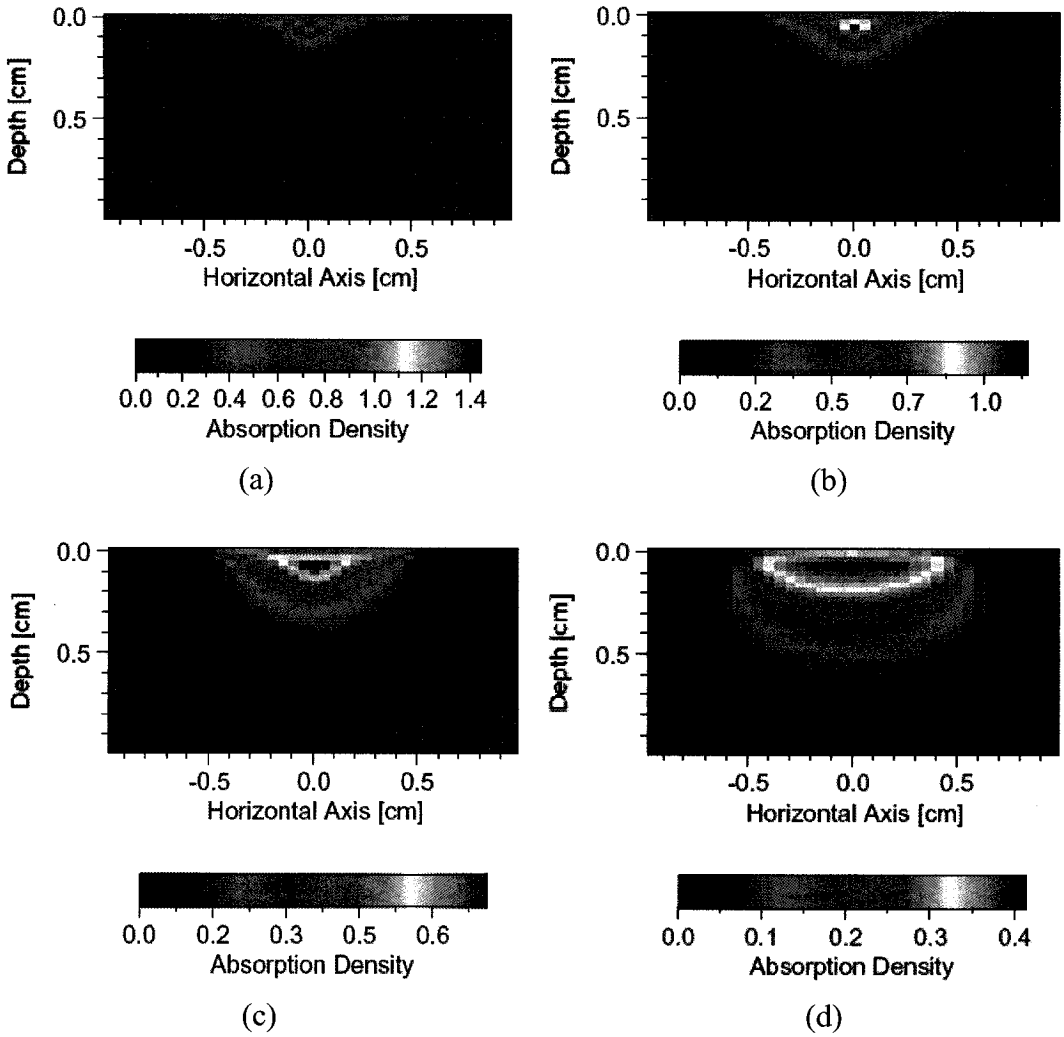

Figure (4-26) Absorption distribution of a uniform intensity focused optical beam in a homogeneous turbid medium under different focusing conditions published in reference [6]. (a) Depth of focal point Z_f=0.05 cm. (b) Depth of focal point Z_f = 0.1 cm. (c) Depth of focal point Z_f = 0.2 cm. (d) Depth of the focal point Z_f=∞ cm. In all cases the radius of the incident optical beam before focusing is 0.5 cm and two million photons are launched in each simulation run.[6]

The differences in calculated results maybe due to the different statistical approaches adapted for tracing of Monte Carlo photons. As mentioned before, our simulation model adapts a variance reduction technique, which is a standard Monte Carlo simulation method for tracing photon movement within the medium. The program written by Wang

and Liang in [6] used a delta-scattering technique to model a different problem in the same study. It needs to be mentioned that reference [6] represents the best available benchmark for testing our program although the programming algorithm differs.

For the sake of making the comparison easy for the reader, the simulation results are rearranged in Figure (4-27). Cases representing the same focusing conditions are shown next to each other.

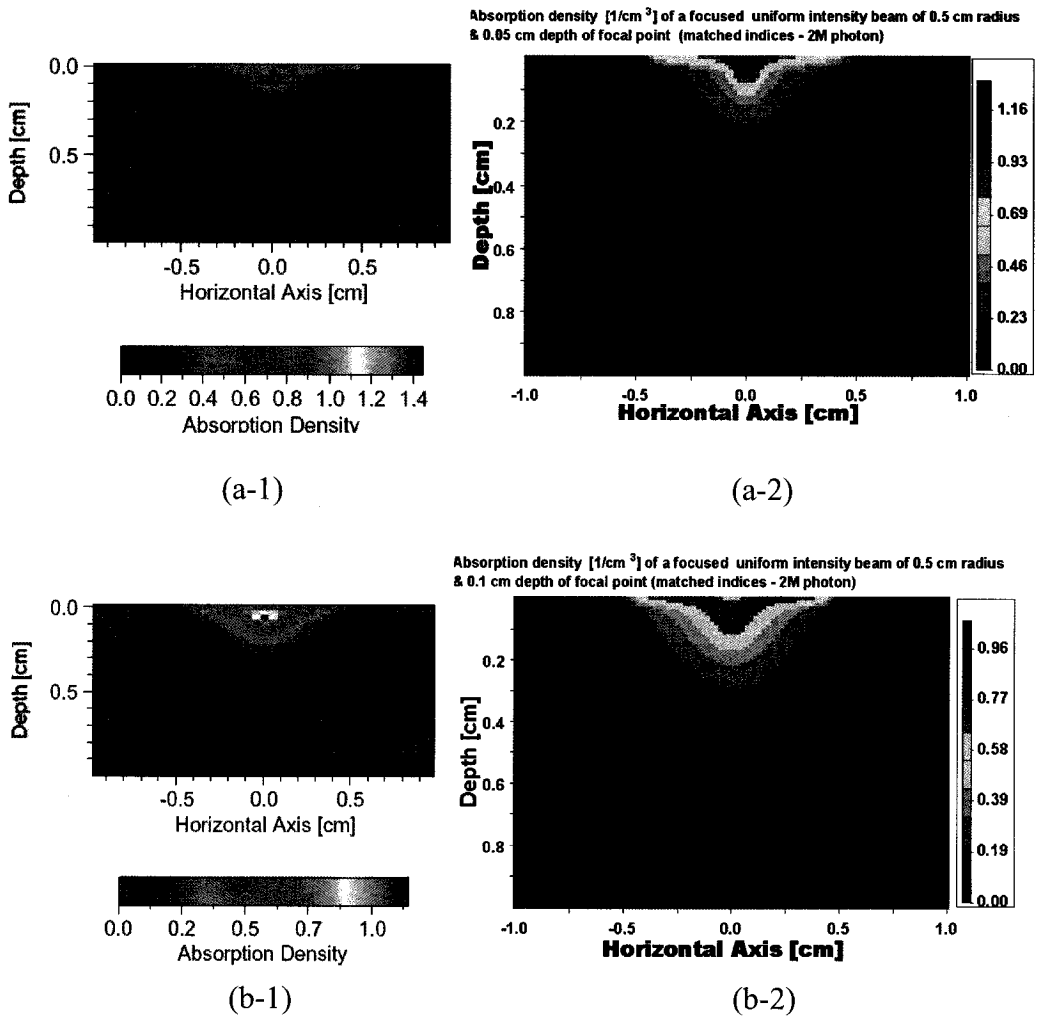

Figure (4-27) Comparison between the simulation results of the absorption distribution of a uniform intensity focused beam in a homogeneous turbid medium under different focusing conditions according to [6] and our model. (a-1) Depth of focal point Z_f=0.05 cm,[6]. (a-2) Depth of focal point Z_f=0.05 cm, our model. (b-1) Depth of focal point Z_f = 0.1 cm, [6]. (b-2) Depth of focal point Z_f = 0.1 cm, our model.

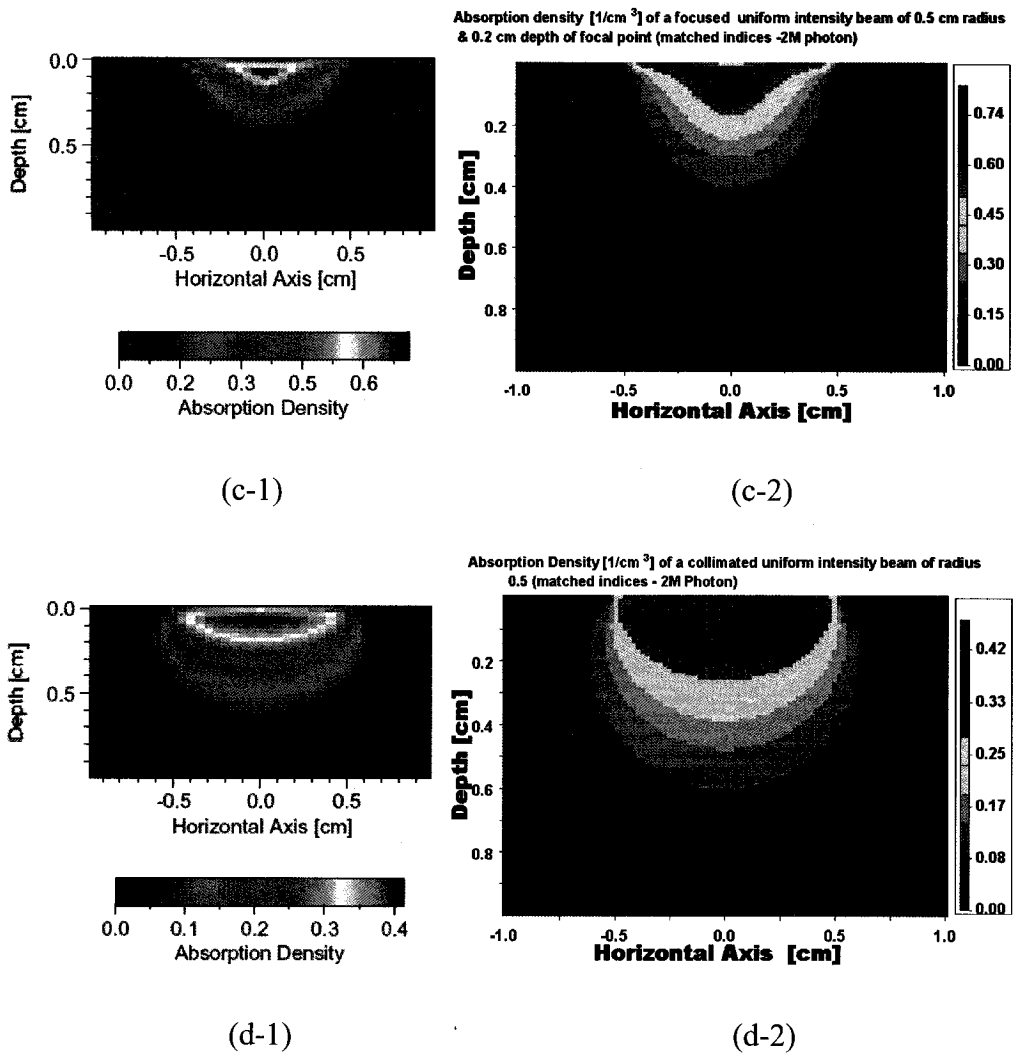

(c-1) (c-2)

(d-1) (d-2)

Figure (4-27) Comparison between the simulation results of the absorption distribution of a uniform intensity focused beam in a homogeneous turbid medium under different focusing conditions according to [6] and our model. (a-1) Depth of focal point Z_f=0.05 cm,[6]. (a-2) Depth of focal point Z_f=0.05 cm, our model. (b-1) Depth of focal point Z_f = 0.1 cm, [6]. (b-2) Depth of focal point Z_f = 0.1 cm, our model. (c-1) Depth of focal point Z_f = 0.2 cm, [6]. (c-2) Depth of focal point Z_f = 0.2 cm, our model. (d-1) Depth of the focal point Z_f=∞ cm, [6]. (d-2) Depth of the focal point Z_f=∞ cm, our model. In all cases the radius of the incident optical beam before focusing is 0.5 cm ($1/e^2$ radius for a Gaussian beam) and two million photons are launched in each simulation run.

In general, it can be seen that the two programs produce very close results of the absorption distribution within the homogeneous turbid medium. In the following chapter the absorption distribution of a focused optical Gaussian beam in the same homogeneous

turbid medium is presented. Then the results of focusing a Gaussian beam into a human skin tissue model are introduced next.

4.3 Summary

In this chapter we verified our model for focusing optical beams into biologically turbid media by means of simulation results comparisons with work produced based on well-established references. Both the accuracy of the sampling rule profiling the optical intensity of a beam and the focusing algorithm adapted were tested by comparison with the best available references in the literature.

CHAPTER 5

Simulation Results of a Focused Gaussian Beam into Multi-Layered Tissue – Case Studies

5.0 Introduction

This chapter introduces two case studies of focusing a Gaussian laser beam into multi-layered tissue. The first case study deals with a single-layer homogenous turbid medium that has exactly the same optical properties of the homogeneous turbid medium discussed in the previous chapter and summarized by table (4-2). The second case study involves a double-layer human skin model studied at two different wavelengths.

5.1 Simulation Results of the Absorption Distribution of a Focused Gaussian Beam into a Homogeneous Turbid Medium

Figure (5-1) below represents the two-dimensional plots of the absorption distribution of a focused Gaussian beam into the homogeneous turbid medium under different focusing conditions. Of course, the depth of the focal point in the turbid medium was taken exactly at the same distances as in the previous section for making the comparison meaningful.

Therefore, the depth of the focal point Z_f was chosen to be 0.05, 0.1, 0.2 and ∞ cm respectively, where ∞ is equivalent to a collimated photon beam. The $1/e^2$ radius of the incident photon beam is 0.5 cm. In all simulation runs, two million photons were launched in order to obtain results with acceptable reduced variance.

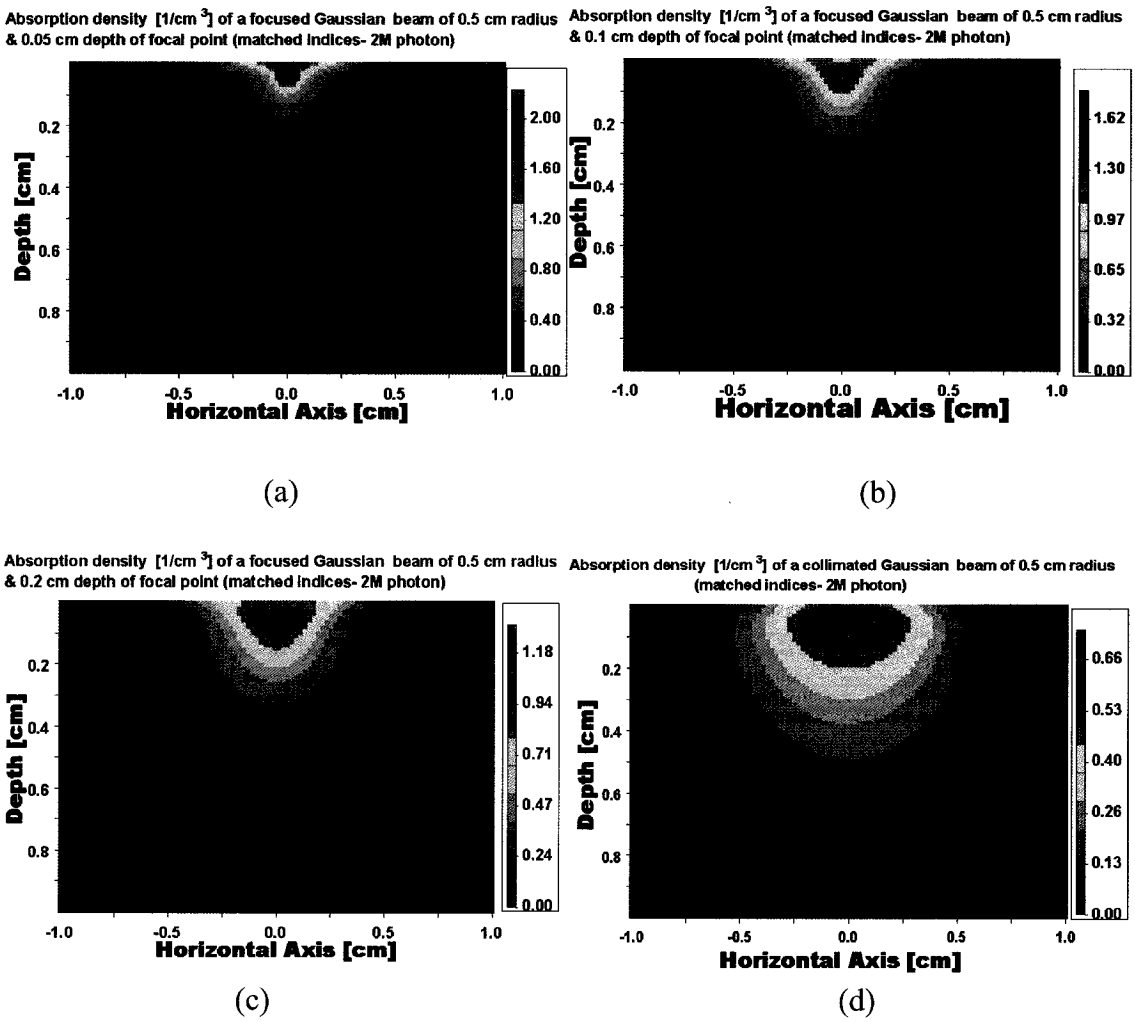

Figure (5-1) Simulation results of the absorption distribution of a focused optical Gaussian beam in a homogeneous turbid medium under different focusing conditions. (a) Depth of focal point Z_f=0.05 cm. (b) Depth of focal point Z_f = 0.1 cm. (c) Depth of focal point Z_f = 0.2 cm. (d) Depth of the focal point Z_f=∞ cm. In all cases the $1/e^2$ radius of the incident optical beam before focusing is 0.5 cm and two million photons are launched in each simulation run.

For convenience, the simulation results for the cases of focused Gaussian beam and focused uniform intensity beam, are rearranged such that the reader can easily compare the absorption density profile for the two beams under the same focusing conditions. The comparison is made clear in figure (5-2) for depths of the focal point of 0.05, 0.1, 0.2 and ∞ cm, respectively.

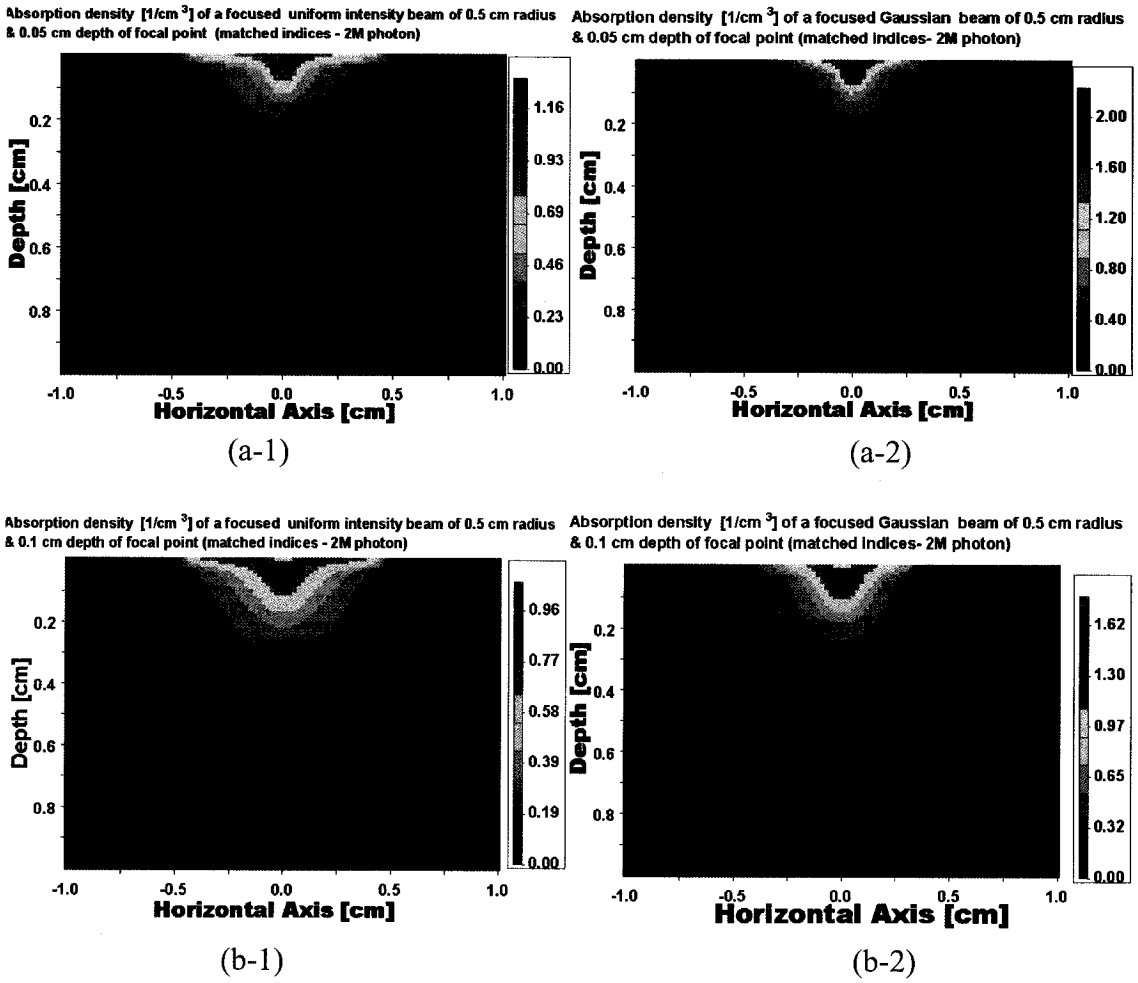

Figure (5-2) Comparison between the simulation results of the absorption distribution of a uniform intensity focused beam and a focused Gaussian beam in a homogeneous turbid medium under different focusing conditions. (a-1) Depth of focal point Z_f=0.05 cm, uniform intensity incident photon beam. (a-2) Depth of focal point Z_f=0.05 cm, Gaussian incident photon beam (b-1) Depth of focal point Z_f = 0.1 cm, uniform intensity incident photon beam. (b-2) Depth of focal point Z_f = 0.1 cm, Gaussian incident photon beam.

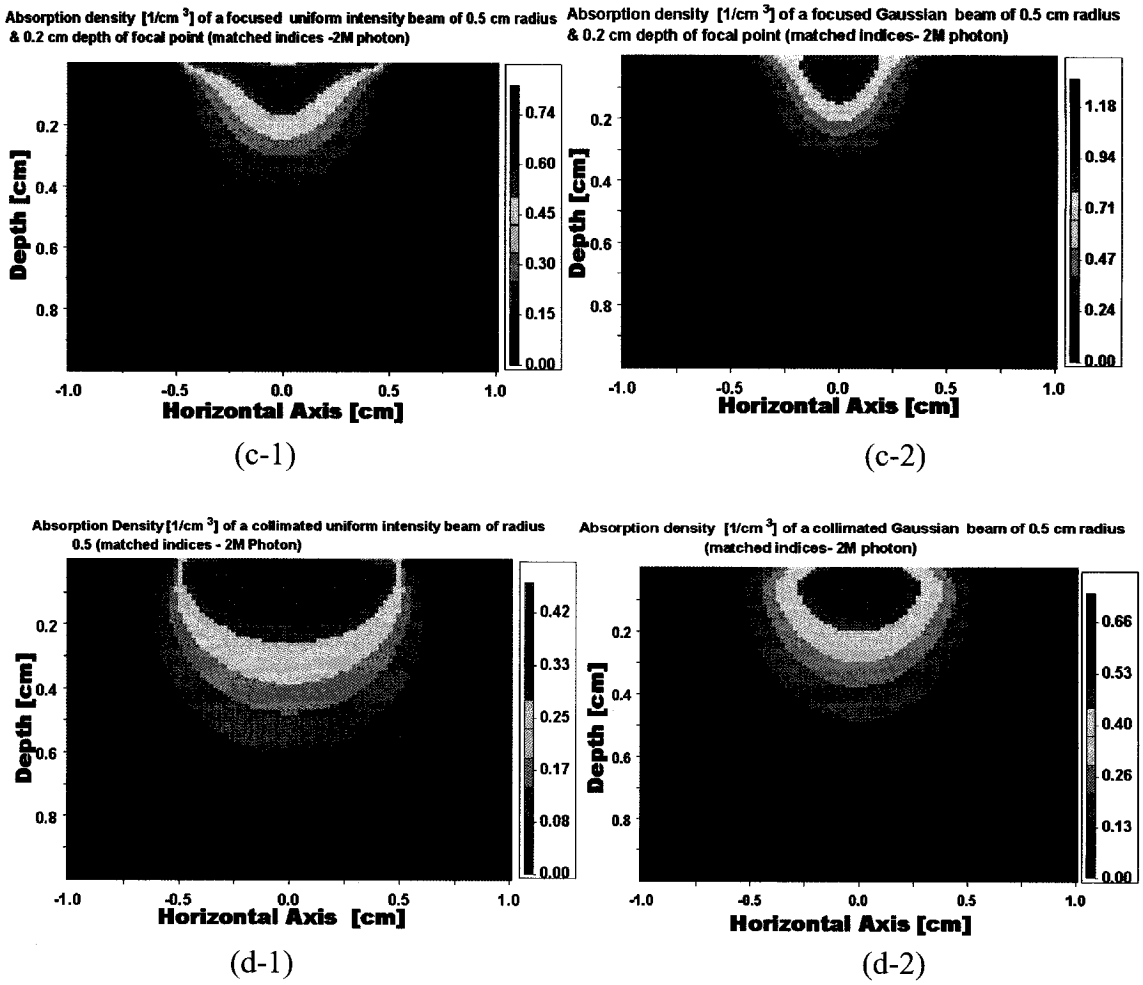

Figure (5-2) Comparison between the simulation results of the absorption distribution of a uniform intensity focused beam and a focused Gaussian beam in a homogeneous turbid medium under different focusing conditions. (c-1) Depth of focal point Z_f = 0.2 cm, uniform intensity incident photon beam. (c-2) Depth of focal point Z_f = 0.2 cm, Gaussian incident photon beam. (d-1) Depth of the focal point $Z_f=\infty$ cm, uniform intensity incident photon beam. (d-2) Depth of the focal point $Z_f=\infty$ cm, Gaussian incident photon beam. In all cases the radius of the incident optical beam before focusing is 0.5 cm ($1/e^2$ radius for a Gaussian beam) and two million photons are launched in each simulation run.

Figure (5-2) reveals some important results concerning modeling laser beams as Gaussian beams when compared with modeling them as uniform intensity beams. It can be seen clearly from the above comparisons that the focused Gaussian beams produce higher absorption density peaks than the corresponding uniform intensity beams. For example, the comparison between figures {5-2 (a-1)} and {5-2 (a-2)} shows that the increase in the

predicted peak absorption density due to the Gaussian beam model is about 42% higher than the corresponding peak absorption density due to the uniform intensity beam model. This result is very important for in some applications such as laser ablation, laser dosimetry and photo-therapy, where absorption density in tissue should be calculated precisely. The comparisons in figure (5-2) also reveals that the spatial distribution of the absorption density profile within the homogeneous turbid medium is more confined in the case of the Gaussian beam model. This feature makes the Gaussian beam model more desirable in terms of photo-therapy applications, where targeting specific area within the biological tissue is important.

5.2 Absorption Distribution of a Focused Gaussian Beam into a Human Skin Tissue Model

In this section a case study of modeling the light absorption density in a human skin model is considered. The Human skin will be modeled as two layers (epidermis and dermis). The first layer (epidermis) has a thickness of 60 μm. The second layer (dermis) is modeled as an infinite homogeneous turbid medium. The optical properties of the human skin were obtained at two different wavelengths of 532 and 1300 nm respectively. The optical properties of the human skin at a wavelength of 532 nm are summarized in table (5-1) as obtained from reference [6]. Table (5-2) summarizes the optical properties of a human skin model at 1300 nm as obtained from reference [32]. It should be noted that the reported optical properties of human skin might vary considerably at comparable wavelengths due to the different tissue origin, preparation, measurement techniques and other factors as well. As a general trend that can be observed for skin tissue samples is the large increase in total attenuation of light due to absorption and scattering in the

ultraviolet region and a decrease in the total attenuation as the wavelength of light increases until a minimum attenuation is noticed between 700-1000 nm [43].

Table (5-1) Optical properties of the human skin tissue model at a wavelength 532 nm. Top and bottom ambient media refractive indices were taken n_a= 1.4 [6].

Layer	Refractive index (n)	Absorption coefficient. cm^{-1}	Scattering Coefficient. cm^{-1}	Anisotropy factor g	Thickness cm
1	1.4	19	480	0.787	0.006
2	1.4	2.2	210	0.787	∞

The wavelength of 532 nm lies in the visible spectral region of light, while the 1300 nm wavelength lies within the near-infrared spectral region of light. This selection of the two wavelengths will give a good chance to study the change in absorption distribution within the human skin model due to the change in the incident wavelength. As seen in figure (5-3), focusing increases the measured peak absorption density as expected. The value of the anisotropy factor (g=0.787) at the 532 nm is more isotropic when compared with the anisotropy factor (g=0.9) at the wavelength of 1300 nm. In general, most of the tissues are highly forward scattering in the near-infrared region [21,22,43,44].

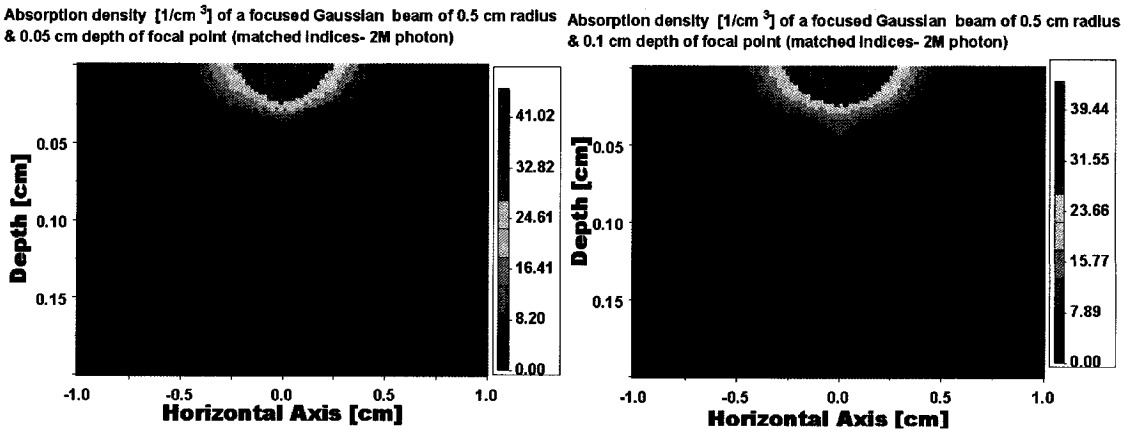

Figure (5-3) Simulation results of the absorption distribution of a focused optical Gaussian beam into a human skin tissue model at a wavelength of 532 nm, under different focusing conditions. (a) Depth of focal point Z_f=0.05 cm. (b) Depth of focal point Z_f = 0.1 cm

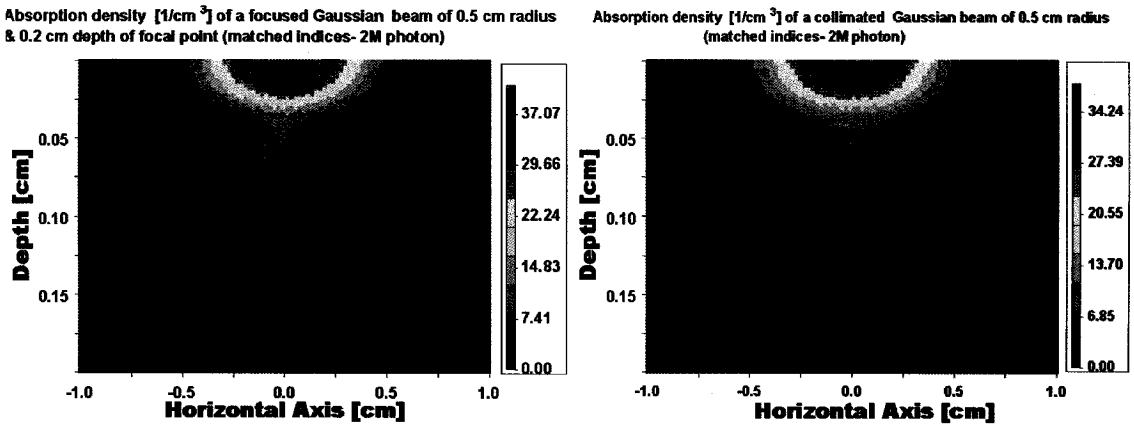

(c) (d)

Figure (5-3) Simulation results of the absorption distribution of a focused optical Gaussian beam into a human skin tissue model at a wavelength of 532 nm, under different focusing conditions (c) Depth of focal point Z_f = 0.2 cm. (d) Depth of the focal point $Z_f=\infty$ cm. In all cases the $1/e^2$ radius of the incident optical beam before focusing is 0.5 cm and two million photons are launched in each simulation run.

Figure (5-4) shows the simulation results of the absorption distribution of a focused Gaussian beam in a human skin tissue model at a wavelength of 1300 nm. For convenience, the results of the simulation runs for the two wavelengths under study were rearranged in order to make the comparison easier for the reader in figure (5-5).

Table (5-2) summarizes the optical properties of the human skin tissue model at a wavelength 1300 nm [32]. The surrounding ambient material on top and on the bottom of the sample under investigation has matched refractive indices with the sample. As it was explained before, this selection is to avoid imposing a Snell's law conditions on the beams entering the tissue. The implementation of such conditions will impose a distortion in the focusing that will be hard to separate from the scattering distortion.

Table (5-2) Optical Properties of the human skin tissue model at a wavelength 1300 nm. Top and bottom ambient media refractive indices were taken n_a= 1.37 [32]

Layer	Refractive index (n)	Absorption coefficient. cm^{-1}	Scattering Coefficient. cm^{-1}	Anisotropy factor g	Thickness cm
1	1.37	10	140	0.9	0.006
2	1.37	1	140	0.9	∞

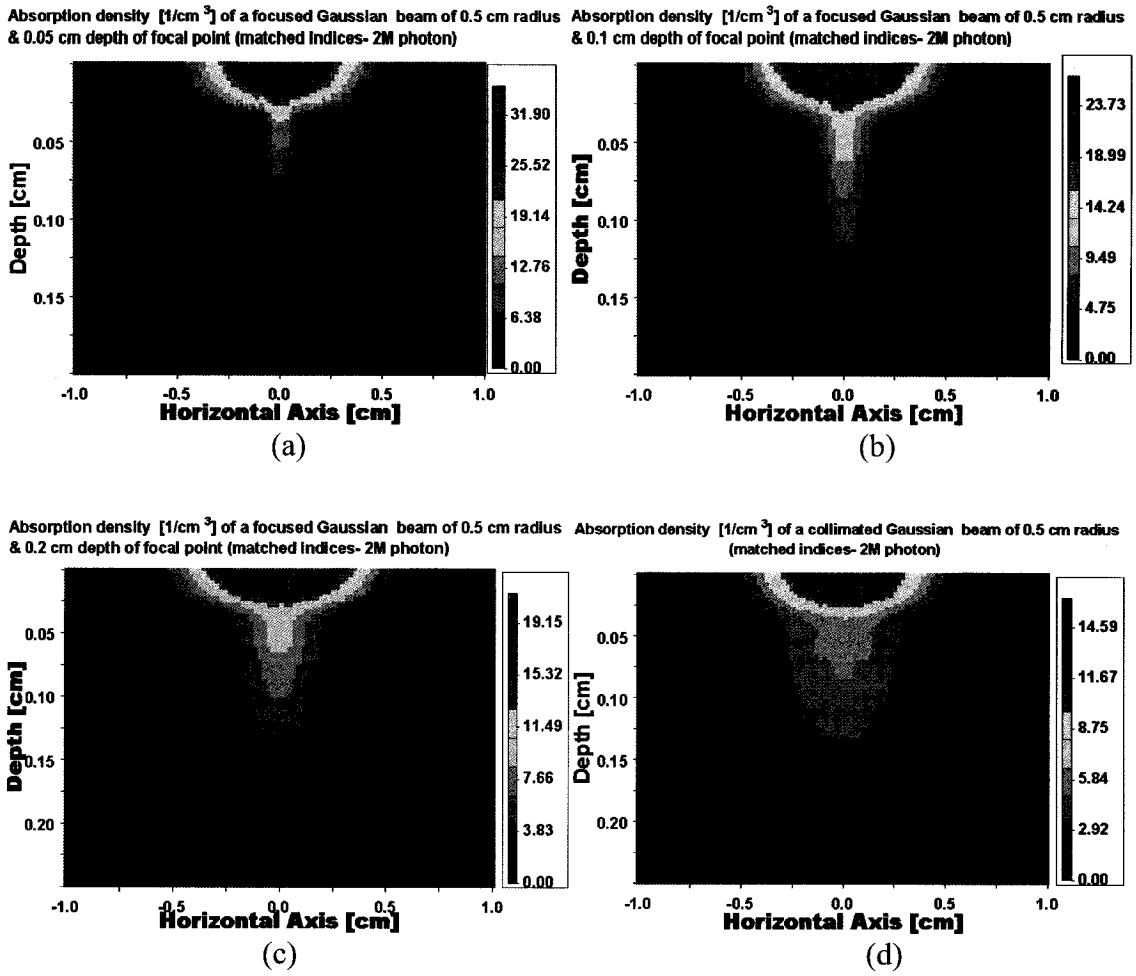

Figure (5-4) Simulation results of the absorption distribution of a focused Gaussian beam into a human skin tissue model at a wavelength of 1300 nm, under different focusing conditions. (a) Depth of focal point Z_f =0.05 cm. (b) Depth of focal point Z_f = 0.1 cm. (c) Depth of focal point Z_f = 0.2 cm. (d) Depth of the focal point Z_f =∞ cm. In all cases the $1/e^2$ radius of the incident optical beam before focusing is 0.5 cm and two million photons are launched in each simulation run.

Comparison between the optical properties of skin model at the two wavelengths in tables (5-1) and (5-2) shows a reduction in the scattering and absorption coefficients at 1300 nm, which makes this wavelength preferable for imaging applications. Around this wavelength, the effect of scattering is reduced compared to wavelengths in the visible region, and the absorption (mainly due to water) is low compared to even longer wavelengths

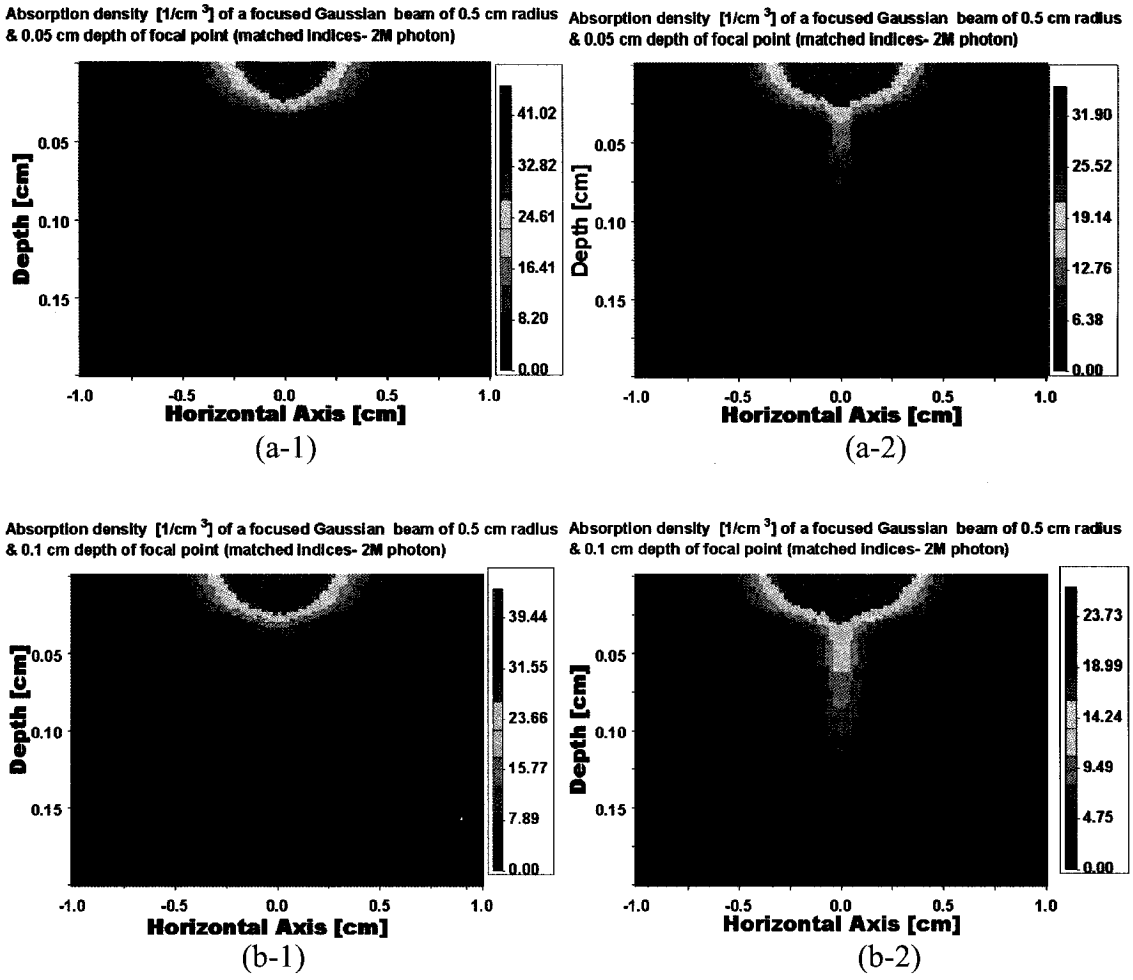

Figure (5-5) Comparison between simulation results of the absorption distribution of a focused Gaussian beam into a human skin tissue model at wavelengths of 532 & 1300 nm, under different focusing conditions. (a-1) Depth of focal point Z_f =0.05 cm, λ=532 nm. (a-2) Depth of focal point Z_f =0.05 cm, λ=1300 nm. (b-1) Depth of focal point Z_f = 0.1 cm, λ=532 nm. (b-2) Depth of focal point Z_f = 0.1 cm, λ=1300 nm

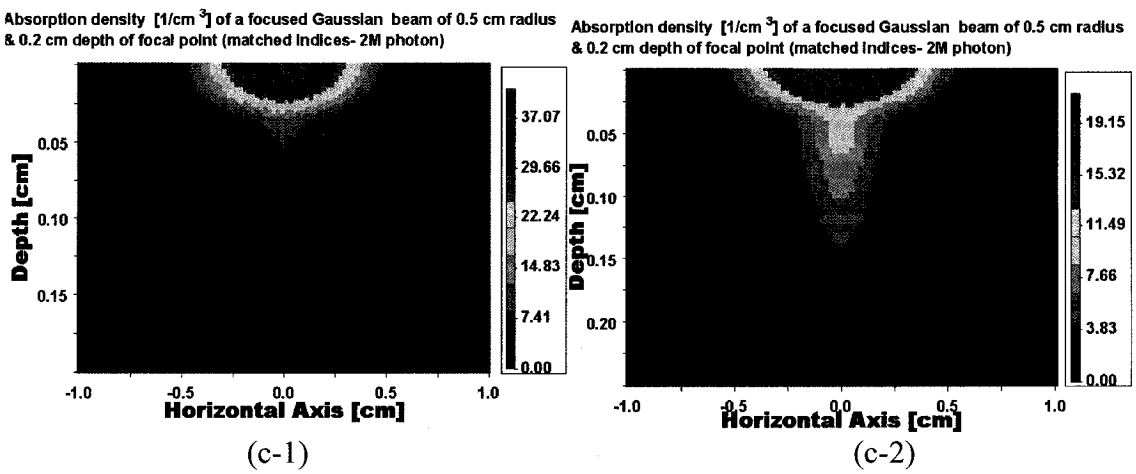

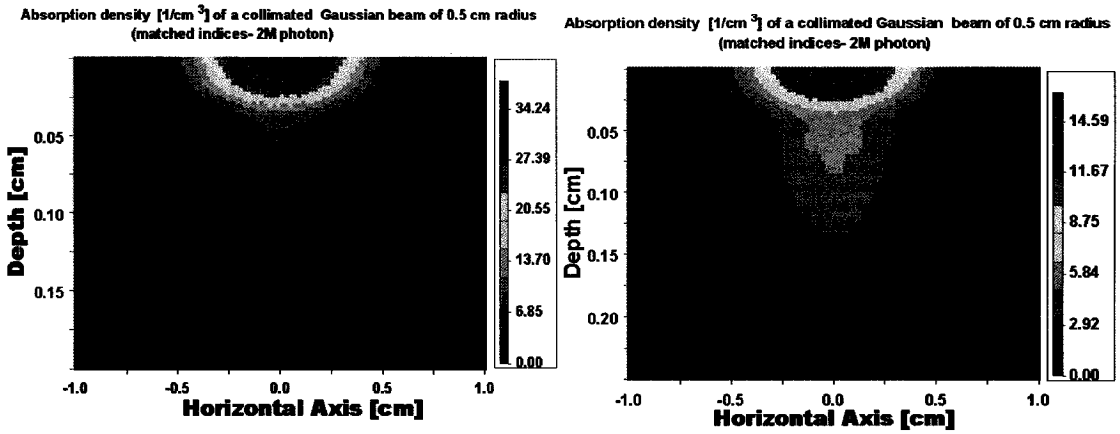

(d-1) (d-2)

Figure (5-5) Comparison between simulation results of the absorption distribution of a focused Gaussian beam into a human skin tissue model at wavelengths of 532 & 1300 nm, under different focusing conditions. (c-1) Depth of focal point Z_f = 0.2 cm, λ=532 nm. (c-2) Depth of focal point Z_f = 0.2 cm, λ=1300 nm. (d-1) Depth of the focal point $Z_f=\infty$ cm, λ= 532 nm. (d-2) Depth of the focal point $Z_f=\infty$ cm, λ= 1300 nm. In all cases the $1/e^2$ radius of the incident optical beam before focusing is 0.5 cm and two million photons are launched in each simulation run.

The comparison between the absorption density in the human skin at 532 & 1300 nm under different focusing conditions that is shown in figure (5-5) confirms some characteristics of human skin previously predicted. For example, a quick comparison between the right (1300 nm wavelength) and left (532 nm wavelength) columns shows the deeper penetration of the longer wavelength in tissue than the shorter wavelength. The absorption profile in general for the 1300 nm wavelength is more directive in the forward direction than the case of 532 nm wavelength. This can be explained if the values of the anisotropy factor (g) in tables (5-1) and (5-2) were examined. The anisotropy factor (g) becomes highly forward scattering (g=0.9) in the 1300 nm region while it is more isotropic at the 532 nm region. In terms of the absorption peak, we notice that using a 532 nm light source can cause the absorption density to be about 29% higher than corresponding absorption density at 1300 nm under the same focusing conditions in

both cases (depth of the focal point is 0.05 cm). This is the case shown in figure {5-5 (a-1) and (a-2)}. For the case of a collimated incident beam as seen in figure {5-5 (d-1) and (d-2)}, an increase of 134% in the peak absorption density at 532 nm over the absorption density due to the same beam at 1300 nm. This result is very interesting. It shows the effect of changing the used wavelength on the optical properties of the biological tissue.

5.3 Summary

This chapter presented all the simulation results obtained in this thesis. These results were divided into two parts. The results in part I served mainly as a verification method for the developed Monte Carlo simulation program for modeling focused optical beams in multi-layered tissues. The simulation results of the proposed Gaussian beam sampling rule (referred to as sampling rule I) are presented and compared with the sampling rule proposed in some references (referred to as sampling rule II). The second part of this chapter, part II, presented two case studies as a direct implementation of the proposed model. The first case study simulated the absorption density distribution in a homogeneous turbid medium due to focusing an optical Gaussian beam into this medium. The second case study in this thesis dealt with the absorption density distribution in a multi-layered human skin tissue model. Results from the two case studies were compared and discussed accordingly.

CHAPTER 6

Conclusion and Outlook

In this thesis we have modeled a focused Gaussian beam with Monte Carlo simulation. The famous "MCML" [25,26] program was modified based on a probability distribution found in the literature. However, errors were encountered in the calculated physical quantities by Monte Carlo simulation. Using simulation, we proved that the probability density function used in the literature is a source of error in the calculations of the physical quantities evaluated by Monte Carlo simulation. We proposed another probability density function that is shown to provide a dramatic improvement compared with the other function. The proposed model of a focused Gaussian beam was applied in two case studies. The first case involved focusing a Gaussian beam into a homogeneous turbid medium and the second case, into a human skin model consisting of two layers. The main conclusions of this research can be summarized in several points as follows:

- The Monte Carlo simulations aim at predicting energy transport in tissue, and although being capable of keeping track of phase and polarization information, it ignores such features during simulation.
- The accurate sampling of a Gaussian beam profile in Monte Carlo method is the key to correctly calculate the scored physical quantities (Absorption, Reflectance and Transmittance) in Monte Carlo modeling of a Gaussian beam incident on multi-layered tissue.
- In the literature, a proposed Gaussian sampling rule described by equation (3-16) and referred to in the thesis as "sampling rule II", was proved to deviate from the calculated physical quantities as calculated by the well established MCML and CONV programs.
- We proved that the sampling rule described by equation (3-14) and referred to as "sampling rule I" in this thesis, describes the Gaussian beam profile in Monte Carlo simulation more accurately as checked against the MCML and CONV programs.
- The error associated with the use of sampling rule II, was found to be related to the intensity of the scored physical quantity. This error increased with the increasing recorded physical quantity and vice versa. This effect can be referred to the dependence of sampling rule II on a normalized probability density function that has different statistical characteristics than the one that is derived from the correct Gaussian intensity profile (sampling rule I) as discussed in section 3.2.

- Because the radial parameter W_b of sampling rule II is actually a normalized beam waist W_o by a factor of $\sqrt{2}$, the error resulting from the use of sampling rule II will be very small in case of Gaussian beams with very small waist and vice versa.
- The focusing process greatly affects the absorption distribution of an optical beam in a homogeneous turbid medium when the depth of the focal point is less than or comparable with the transport mean free path.
- Focusing of Gaussian beams into a homogeneous turbid medium results in an increased peak absorption density comparable with the case of a focused uniform intensity photon beam under the same focusing conditions.
- The spatial absorption distribution resulting from focusing a Gaussian beam into a homogeneous turbid medium is more confined than the spatial absorption distribution resulting from focusing a uniform intensity photon beam into the same medium. In terms of photo-therapy applications, this is a desirable characteristic in targeting specific area within the biological tissue.

The future directions of the research work done in this thesis can be summarized as follows:

- Based on the proposed Monte Carlo Gaussian sampling rule in this thesis, improvement of the focusing model can be realized by adapting other focusing methods rather than the geometric-focus. A spot focus method or a hyperboloid method recently suggested by a research group [31] can be used to model the focusing of optical beams in general. Comparisons among different approaches can suggest the most accurate method to use.

- This study constitutes a building block for modeling Optical Coherence Tomography systems [45], which usually involve focusing of optical beams into tissue. These imaging systems are based on detecting single scattered photons from biological tissue layers as diffuse reflectance. Modeling the heterodyne detection and applying a suitable detection criterion for detecting single scattered photons, along with modeling of focused optical beams, can model the Optical Coherence Tomography system by Monte Carlo simulation. Based on the proposed Monte Carlo Gaussian sampling rule in this thesis (sampling rule I), the Optical Coherence Tomography system can be compared with an existing model [31] that adapted the Gaussian sampling rule II. It should be clear that the imaging applications in general usually process back reflected or back scattered light of tissue layers. In this thesis we introduced a model for focusing optical beams into multi-layered tissue that was verified mainly by comparison of other physical quantity, namely absorption. This approach was adapted due to the difficulty in finding reference data for making comparisons. This is mainly due to the statistical nature of the Monte Carlo method, which makes comparison with references and experimental data the main method for verification of Monte Carlo models.

REFERENCES

[1] Paras. N. Prasad, *Introduction to Biophotonics*, (John Wiley&Sons, 2003).

[2] E. Viherkoski, "Lasers in medicine", Annales Chirurgiae et Gynecologiae **79,** 176-181 (1990).

[3] A. Enejder, "Light scattering and absorption of tissue- models and measurements", Ph.D. dissertation, Lund Institute of Technology, Sweden (1997).

[4] S. L. Jacques, "Laser-tissue interactions, photochemical, photothermal, and photomechanical," Lasers in General Surgery **72,** 531-558 (1992).

[5] S. Chandrasekhar, *Radiative Transfer*, (New York: Dover, 1960).

[6] L. V. Wang and G. Liang, "Absorption distribution of an optical beam focused into a turbid medium" Applied Optics,**38**, 4951-4958, (1999).

[7] N. Metropolis and S. Ulam, " *The Monte Carlo method*", J. Am. Statistical Association, **44**,335,341, (1949).

[8] H. Kahn and T.E. Harris , "Estimation of particle transmission by random sampling in Monte Carlo Method", Vol **12** of National Bureau of Standards Applied Mathematics Series, 27-30, (U.S. Government Printing Office , Washington ,D.C., 1951).

[9] B.C. Wilson and G. Adam," A Monte Carlo for absorption and flux distributions of light in tissue," Med. Phys., **10**, 842-830, (1983).

[10] S. A. Prahl, M. Keijzer, S. L. Jacques, A. J. Welch, "A Monte Carlo Model of Light Propagation in Tissue", Dosimetry of Laser Radiation in Medicine and Biology SPIE Institute Series Vol. IS **5**, 102- 111, (1989)

[11] S. Prahl , " Light Transport in Tissue", Ph.D. dissertation ,The University of Texas at Austin, (1988).

[12] C. F. Bohren and D. R. Huffman, *Absorption and scattering of light by small particles,* (John Wiley & Sons, Inc., New York, NY 1983).

[13] M. J. C. Van Gemert, S. L. Jacques, H. J. C. M. Sterenborg, and W. M. Star, " Skin Optics", IEEE Transactions on biomedical engineering, **36**, 1146-1154, (1989).

[14] S. T. Flock, B. C. Wilson, and M. S. Patterson, "Monte Carlo modeling of light propagation in highly scattering tissue - II: Comparison with measurements in phantoms", IEEE Trans. Biomed. Eng. **36,** 1169-1173 (1989).

[15] Claes af klinteberg, "On the use of light for the characterization and treatment of malignant tumors", Doctoral Thesis, Lund Institute of Technology, (1999).

[16] S.L. Jacques and S. Prahl, Oregon medical laser center website, http://omlc.ogi.edu.

[17] J. M. Schmitt and G. Kumar, "Turbulent nature of refractive index variation in biological tissue", Opt Lett. **21**, 1310-1312, (1996).

[18] Ed. A. J. Welch and M. J. C. van Gemert, *Optical-thermal response of laser-irradiated tissue.* (Plenum, New York: 1995).

[19] S. L. Jacques et al., "Angular Dependence of HeNe Laser Light Scattering by Human Dermis", Lasers in the Life Science 1(4), pp. 309-334, (1987).

[20] L.G. Henyey and J.L. Greenstein, "Diffuse radiation in the galaxy", Astrophys. J. **93**, 70-83, (1941).

[21] G. Yoon, A. J. Welch, M. Motamedi, and M. J. C. van Gemert, "Development and application of three dimensional light distribution model for laser irradiated tissue," IEEE J. Quant. Electr. **QE-23,** 1721-1733 (1987).

[22] M. R. Arnfield, J. Tulip, and M. S. McPhee, "Optical propagation in tissue with anisotropic scattering," IEEE Trans. Biomed. Eng. **35,** 372-381 (1988).

[23] I. Lux and L. Koblinger, "Monte Carlo Particle Transport Methods: Neutron and Photon Calculations" ,CRC Press, Boca Raton, Fla., (1991).

[24] Kahn, H., "Applications of Monte Carlo", AECU-3259 Report, Rand Corporation, Santa Monica, CA, 1954.

[25] L.-H. Wang, S. L. Jacques, and L.-Q. Zheng, "MCML - Monte Carlo modeling of photon transport in multi-layered tissues," Computer Methods and Programs in Biomedicine **47**, 131-146,(1995).

[26] L.-H. Wang and S. L. Jacques, *Monte Carlo Modeling of Light Transport in Multi-layered Tissues in Standard C*, (University of Texas M. D. Anderson Cancer Center,1992)

[27] L.-H. Wang, S. L. Jacques, and L.-Q. Zheng, "CONV – Convolution for responses to a finite diameter photon beam incident on multi-layered tissues," Computer Methods and Programs in Biomedicine **54**, 141-150, (1997).

[28] Kalos M.H., and P.A. Whitlock, "Monte Carlo Methods, I: Basics," John Wiley & Sons, Inc. (1986).

[29] A. Siegman , *Lasers*, (University Science Books,1986).

[30] B.A. Saleh and M.C. Teich, *Fundamentals of Photonics*, (John Wiley & Sons, Inc., 1991).

[31] A. Tycho, T.M. Jorgensen, H.T. Yura and P.E. Andersen, "Derivation of a Monte Carlo method for modeling heterodyne detection in optical coherence tomography systems", Applied. Opt. **41**,6676-6691, (2002).

[32] A. Tycho, "Optical Coherence Tomography: Monte Carlo Simulation and Improvement by Optical Amplification", Ph.D. Thesis, Technical University of Denmark, (2002).

[33] Z. Song, K Dong, X.H. Hu, and J.Q. Lu " Monte Carlo simulation of converging laser beams propagating in biological materials", Applied Optics, **38**, 2944 – 2949, (1999).

[34] D. J. Smithies , Tore Lindmoyz, Zhongping Cheny, J Stuart Nelsony andThomas E Milnery, "Signal attenuation and localization in optical coherence tomography studied by Monte Carlo simulation", Phys. Med. Biol. **43**, 3025–3044, (1998)

[35] A.K. Dunn, C. Smithpeter, A. J. Welch,and R. Ritchards- Kortum, " Sources of contrast in confocal reflectance imaging", Applied Optics, **35**, 3441-3446, (1996).

[36] L.Thrane. "Optical Coherence Tomography : Modeling and Applictions", Ph.D. Thesis , Risø National Laboratory, Roskilde, Denmark, (2001).

[37] P. Andersen Lars Thrane, Harold T Yura, Andreas Tycho, Thomas M Jørgensen and Michael H Frosz1, "Advanced modeling of optical coherence tomography systems" Phys. Med. Biol. **49,** 1307–1327, (2004)

[38] J.M. Smith and K. Ben-Letaief, "Efficient Monte Carlo simulation of confocal microscopy in biological tissue", J. Opt. Soc. Am. A **13**, 952-961, (1996).

[39] J. Smith , A Knuttel, and M. Yadloweski "Confocal microscopy in turbid medium", J. Opt. Soc. Am. A **11**, 2226-2235,(1994).

[40] C. M. Blanca and Caesar Saloma, "Monte Carlo analysis of two-photon fluorescence imaging through a scattering medium", Applied Optics, **37**, 8092-8102, (1998).

[41] C.M. Blanca and C. Saloma, " Efficient analysis of temporal broadening of a pulsed focused Gaussian beam in scattering media", Applied Optics, 38 , 5433-5437, (1999).

[42] Willem M Star, "Light dosimetry *in vivo*", Phys. Med. Biol. **42**, 763–787, (1997).

[43] B. Bouma and G. Tearney, *Handbook of Optical Coherence Tomography*,(Marcel Dekker Inc.,2002)

[44] W. Cheong, S. A. Prahl, and A. J. Welch, " A review of the optical properties of biological Tissues", IEEE J. Quantum Electron. ,**26**, 2166-2185, (1990).

[45] Huang, David, Swanson, Eric A, CharlesP. Lin; Joel S. Schuman, William G. Stinson, Warren Chang, Michel R. Hee, Thomas Flotte, Kenton Gregory, Carmen A. Puliafito, James G. Fujimoto, "Optical Coherence Tomography",Science; **254**, 5035;1178-1181,1991.